Journal of Medicinal Chemistry

Article

Cite This: J. Med. Chem. 2019, 62, 2083−2098

pubs.acs.org/jmc

Exploiting the Tolerant Region I of the Non-Nucleoside Reverse Transcriptase Inhibitor (NNRTI) Binding Pocket: Discovery of Potent Diarylpyrimidine-Typed HIV-1 NNRTIs against Wild-Type and E138K Mutant Virus with Significantly Improved Water Solubility and Favorable Safety Profiles

Boshi Huang,[†,⊥] Wenmin Chen,[†,#] Tong Zhao,[†] Zhenyu Li,[‡] Xiangyi Jiang,[†] Tiziana Ginex,[§] David Vílchez,[§] Francisco Javier Luque,[§] Dongwei Kang,[†] Ping Gao,[†] Jian Zhang,[†] Ye Tian,[†] Dirk Daelemans,[∥] Erik De Clercq,[∥] Christophe Pannecouque,[*,∥] Peng Zhan,[*,†] and Xinyong Liu[*,†]

[†]Department of Medicinal Chemistry, Key Laboratory of Chemical Biology (Ministry of Education), School of Pharmaceutical Sciences, Shandong University, 44 West Culture Road, 250012 Jinan, Shandong, PR China

[‡]Department of Pharmacy, Shandong Provincial Hospital Affiliated to Shandong University, Jinan 250021 Shandong, China

[§]Department of Nutrition, Food Science and Gastronomy, Faculty of Pharmacy, Campus Torribera, Institute of Biomedicine (IBUB) and Institute of Theoretical and Computational Chemistry (IQTCUB), University of Barcelona, 08921 Santa Coloma de Gramenet, Spain

[∥]Rega Institute for Medical Research, Laboratory of Virology and Chemotherapy, K.U. Leuven, Herestraat 49 Postbus 1043 (09.A097), B-3000 Leuven, Belgium

Supporting Information

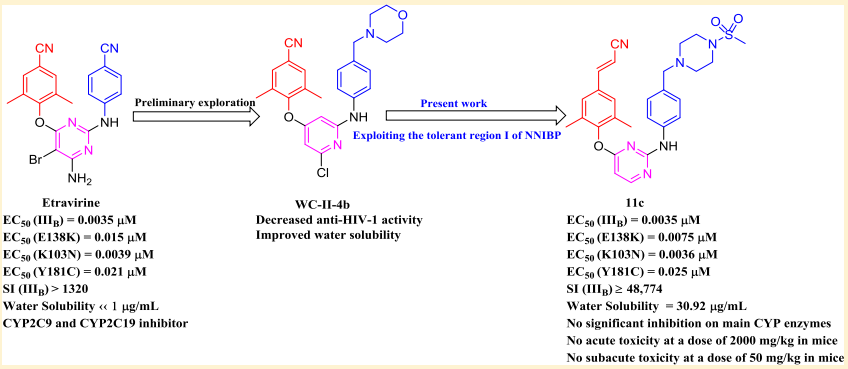

ABSTRACT: Diarylpyrimidine derivatives (DAPYs) exhibit robust anti-HIV-1 potency, although they have been compromised by E138K variant and severe side-effects and been suffering from poor water solubility. In the present work, hydrophilic morpholine or methylsulfonyl and sulfamide-substituted piperazine/piperidines were introduced into the right wing of DAPYs targeting the solvent-exposed tolerant region I. The anti-HIV-1 activities of **11c** ($EC_{50(WT)}$ = 0.0035 μM, $EC_{50(E138K)}$ = 0.0075 μM) were the same as and 2-fold better than that of the lead etravirine against the wild-type and E138K mutant HIV-1, respectively, with a relative low cytotoxicity ($CC_{50} \geq 173$ μM). Further test showed a significant improvement in the water solubility of **11c**. Besides, **11c** displayed no significant inhibition on main cytochrome P450 enzymes and exhibited no acute/subacute toxicities at doses of 2000 mg·kg^{-1}/50 mg·kg^{-1} in mice. Taken together, we consider that **11c** is a promising lead for further structural optimization.

INTRODUCTION

HIV-1 non-nucleoside reverse transcriptase inhibitors (NNRTIs), which disrupt the normal functions of RT via binding to NNRTI binding pocket (NNIBP) close to the polymerase active site,[1] have been a vital component of highly active antiretroviral therapy (HAART) for the treatment of HIV-1 infection.[2] Unfortunately, the clinical application of NNRTIs is seriously compromised by rapid emergence of HIV-1 drug-resistant variants.[3]

In arduous efforts to develop next-generation NNRTIs with improved antidrug resistance profiles, etravirine (ETR, TMC125) and rilpivirine (RPV, TMC278) (Figure 1) have

Received: November 6, 2018
Published: February 5, 2019

DOI: 10.1021/acs.jmedchem.8b01729
J. Med. Chem. 2019, 62, 2083−2098

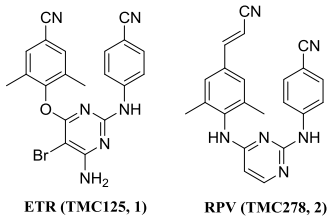

Figure 1. Chemical structures of DAPY-typed NNRTI drugs.

been approved by U.S. FDA in 2008 and 2011, respectively.[4] Both of them belong to diarylpyrimidine (DAPYs) derivatives and show robust antiviral potency against wild-type (WT) and mutant HIV-1 strains at nanomolar concentrations.[5] However, DAPYs have been suffering from poor solubility.[6] ETR is practically insoluble in water over a wide pH range ($\ll$1 μg/mL at pH 7.0), leading to a daily dosage of 400 mg due to extensive formulation work. Besides, the absolute oral bioavailability of ETR in human is still unknown. RPV is hardly dissolved in water (20 ng/mL at pH 7.0), which makes it to display an atypical absorption mechanism involving aggregates. The daily dosage for another NNRTI drug nevirapine (NVP) is 400 mg as for ETR, whereas its antiviral activity against WT HIV-1 strain is approximately 100-fold less than that of ETR. Undoubtedly, a crucial factor is that the aqueous solubility of NVP is 167 μg/mL.[7] The low solubility of DAPYs was therefore identified as an intractable issue to address.

Moreover, Steegen et al. found that only about one-third of patients could retain full susceptibility to the two DAPY drugs (for ETR, 36.5%; for RPV, 27.3%).[8] Among the NNRTI resistance-associated mutations (RAMs), E138K substitution in RT is the first of these ETR selected mutations in B and non-B HIV-1 subtypes (non-B subtype infections represent >90% of the global HIV problem), and is also the most prevalent single mutation found in patients who failed RPV-containing therapy.[9,10] E138K mutation confers phenotypic resistance to the first-generation NNRTIs NVP and efavirenz (EFV) as well.[11] The broad cross-resistance profiles against almost all of the NNRTI drugs indicate that the development of E138K must be restrained whenever possible.[12] In addition, ETR shows severe side-effects, such as peripheral neuropathy, skin rash, and hepatotoxicity, which was ever listed as "dangerous drugs" by U.S. FDA in 2008. Thus, it is still urgently needed to identify novel DAPY-typed HIV-1 NNRTIs endowed with high potency against WT and resistance-associated variants especially E138K, as well as with improved water solubility and favorable safety profiles.

The crystallographic studies of DAPYs showed that the right aminobenzonitrile motif pointed to a rather plastic "groove" of NNIBP, termed as tolerant region I. This open tolerant region, composed of V106, F227, Y318, and P236 residues of the binding pocket, is extended to the RT/solvent interface and could well accommodate diverse substituents (Figure 2).[13] Introduction of polar or hydrophilic substituents, such as morpholine, piperazine, and piperidine, into the right wing of DAPYs around the tolerant region I may contribute to improvement of solubility or pharmacokinetic properties. Based on this analysis, we previously synthesized a series of morpholine-substituted pyridine-type DAPY derivatives. However, the most active inhibitor **WC-II-4b** exhibited decreased activity against WT HIV-1 strain compared to that of ETR and was totally inactive against the most frequently encountered K103N/Y181C double mutant HIV-1 strain, though it

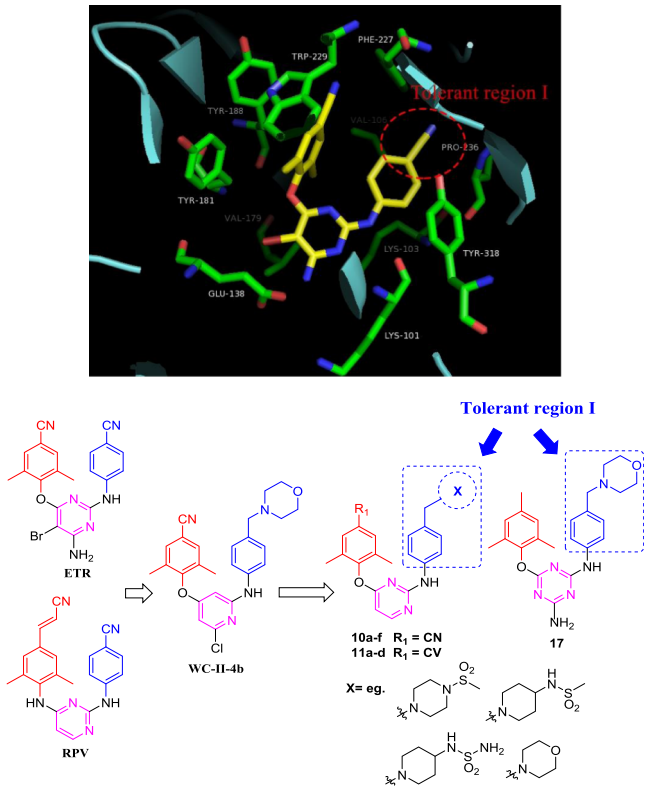

Figure 2. Illustration of the tolerant region I in NNIBP (cocrystal structure of ETR/RT, PDB code: 3MEC) and flowchart summarizing the discovery and optimization strategy for novel DAPY-typed HIV-1 NNRTIs targeting the tolerant region I of NNIBP. The figure of the cocrystal structure of ETR/RT was generated using PyMOL (www.pymol.org).

demonstrated enhanced solubility.[13] We speculated that lack of polar interactions between the right wing of the inhibitor and the surrounding residues of tolerant region I lead to unsatisfactory anti-HIV activity.

Additionally, we found that methylsulfonyl and sulfamide functional groups were adaptive substituents around the tolerant region I according to previously extensive studies.[14,15] They are highly polar and prone to accepting or donating a proton (for sulfamide), resulting in readily forming potential hydrogen bonding interactions with RT.

In the present study, hydrophilic morpholine or methylsulfonyl and sulfamide-substituted piperazine/piperidines were introduced into the right wing of DAPYs targeting the tolerant region I of NNIBP for the first time. The privileged pyrimidine or triazine was employed as the core ring in these new derivatives, which was expected to anchor functional groups and act as a hydrogen bond acceptor to form crucial hydrogen bonding interaction with K101. Meanwhile, the preferred 2,4,6-trisubstitued moiety of DAPYs was installed at the left-wing portion. We expected that the newly introduced hydrophilic motif could form additional interactions (most possibly hydrogen bonding interactions) with the surrounding residues of the tolerant region I, aiming at the identification of compounds with maintained or even higher potency against WT and drug-resistant HIV-1 strains as well as improved water solubility (Figure 2). Herein, we report the multidimensional optimization, preliminary structure−activity relationships (SARs), modeling simulation study, solubility measurement, inhibitory effects on CYP enzymes, and acute/subacute toxicity

DOI: 10.1021/acs.jmedchem.8b01729
J. Med. Chem. 2019, 62, 2083−2098

assessment results of the newly designed DAPY-typed derivatives.

CHEMISTRY

The synthetic protocols for the newly designed derivatives are depicted in Schemes 1, 2, 3 and 4. First, intermediates **5a−d** were prepared from 4-nitrobenzyl bromide (**3**) via a nucleophilic substitution with morpholine or substituted piperazine/piperidines and followed by reduction of the nitro group to the amino group in the presence of stannous chloride.[13] Intermediate **7** (*tert*-butyl(chlorosulfonyl)carbamate) was obtained through treating chlorosulfonyl isocyanate with *t*-BuOH.[16] Next, the starting material 2,4-dichloropyrimidine (**8**) was undergone a nucleophilic substitution reaction with 4-hydroxy-3,5-dimethylbenzonitrile or (*E*)-3-(4-hydroxy-3,5-dimethylphenyl)acrylonitrile to give the key intermediates **9a−b**, followed by a Buchwald−Hartwig reaction with prepared **5a−d**, providing part of the target compounds **10a−c** and **11a−b**.[17] Subsequent deprotection of the Boc group afforded intermediates **12a−d**,[18] which were finally treated with methanesulfonyl chloride to offer the target compounds **10d−e** and **11c−d**.[19] Additionally, treatment of **12b** with intermediate **7** in the presence of triethylamine yielded the Boc-protected intermediate **13**, which was also deprotected to supply the final product **10f**. Similarly, the starting material 2,4,6-trichloro-1,3,5-triazine (**14**) was undergone successive nucleophilic substitution reactions and one-step aminating reaction[20] to provide the target compound **17**. All the novel DAPY-typed derivatives were fully characterized by means of high resolution mass spectrometry (HRMS), proton nuclear magnetic resonance (^{1}H NMR), and carbon nuclear magnetic resonance (^{13}C NMR).

Scheme 1[a]

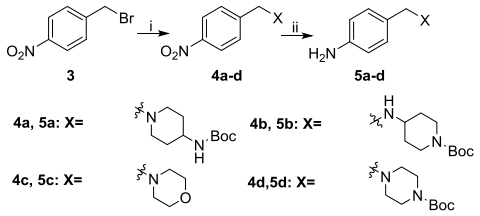

[a]Reagents and conditions: (i) TEA, DCM, rt; (ii) $SnCl_2{\cdot}2H_2O$, EtOH, N_2, rt.

Scheme 2[a]

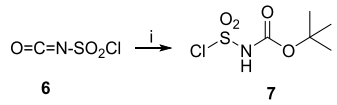

[a]Reagents and conditions: (i) *t*-BuOH, DCM, 0 °C.

Scheme 4[a]

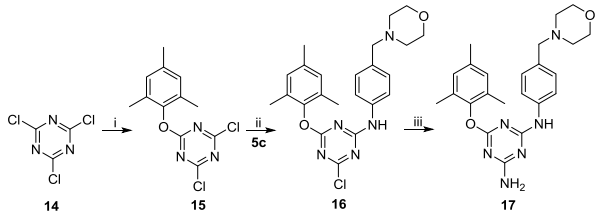

[a]Reagents and conditions: (i) 2,4,6-trimethylphenol, K_2CO_3, DMF, 50 °C; (ii) **5c**, $NaHCO_3$, THF/acetone/water, 30 °C; (iii) $NH_3{\cdot}H_2O$, 1,4-dioxane, sealed tube, 100 °C.

RESULTS AND DISCUSSION

Antiviral and HIV-1 RT Inhibitory Activities and SAR Analysis. All synthesized compounds were evaluated for their anti-HIV activity and cytotoxicity using the MTT method in MT-4 cells infected with WT HIV-1 strain (III_B) and K103N/Y181C double mutant HIV-1 strain (RES056), as well as HIV-2 strain (ROD).[22] Selected compounds were further biologically evaluated for their inhibitory activity against E138K and a panel of other drug-resistant single- and double-mutant strains, including L100I, K103N, Y181C, Y188L, and F227L + V106A. Five approved drugs, lamividine (3TC), zidovudine (AZT), NVP, EFV, and ETR, were used as controls. The

Scheme 3[a]

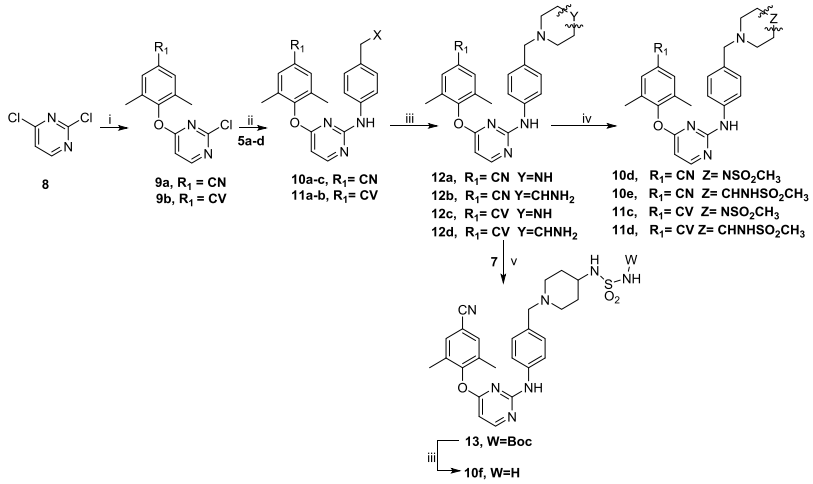

[a]Reagents and conditions: (i) 4-hydroxy-3,5-dimethylbenzonitrile or (*E*)-3-(4-hydroxy-3,5-dimethylphenyl)acrylonitrile, K_2CO_3, DMF, 50 °C; (ii) **5a−d**, $Pd(OAc)_2$, xantphos, Cs_2CO_3, N_2 atmosphere, 1,4-dioxane, 90 °C; (iii) TFA, DCM, rt; (iv) $ClSO_2CH_3$, TEA, DCM, rt (v) 7, TEA, DCM, rt.

DOI: 10.1021/acs.jmedchem.8b01729
J. Med. Chem. 2019, 62, 2083−2098

Table 1. Antiviral Activity against HIV-1 III_B and RES056 Strains and Cytotoxicity of the Target Compounds in MT-4 Cells

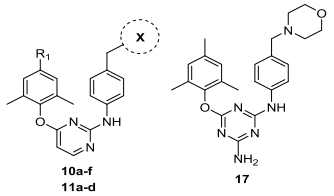

			EC_{50} (μM)[a]			SI[c]	
Compds	R_1	X	III_B	RES056	CC_{50} (μM)[b]	III_B	RES056
10a	CN		0.20 ± 0.019	> 4. 34	4. 34 ± 1.09	21	<1
10b	CN	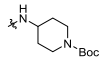	0.19 ± 0.011	> 3.51	3.51 ± 1.47	19	<1
10c	CN		0.011 ± 0.0015	> 23.0	23.0 ± 7.30	2042	<1
10d	CN		0.0072 ± 0.0029	> 3.43	3.43 ± 2.03	475	<1
10e	CN		0.055 ± 0.014	> 18.1	18.1 ± 6.98	331	<1
10f	CN	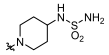	0.092 ± 0.045	> 3.72	3.72 ± 1.37	40	<1
11a	CV[d]		0.015 ± 0.0088	> 3.04	3.04 ± 1.05	209	<1
11b	CV		0.026 ± 0.017	> 3.55	3.55 ± 1.15	138	<1
11c	CV		0.0035 ± 0.00075	0.79 ± 0.026	≥ 173	≥ 48,774	≥ 219
11d	CV		0.0069 ± 0.0015	> 6.99	6.99 ± 5.93	1019	<1
17			0.12 ± 0.034	> 12.89	≥ 12.89	≥ 105	<orX1[e]
WC-II-4b[f]			0.93 ± 0.6	> 6.9	7.0 ± 2.9	7	<1
3TC			6.41 ± 0.37	ND[g]	> 87.2	> 14	ND
AZT			0.011 ± 0.0016	0.015 ± 0.0044	> 7.48	>704	>515
NVP			0.24 ± 0.024	> 15.0	> 15.0	> 62	X1
EFV			0.0013 ± 0.00032	0.24 ± 0.032	> 6.34	> 4969	> 26
ETR			0.0035 ± 0.00018	0.050 ± 0.000	> 4.59	> 1320	> 92
RPV[h]			0.0013 ± 0.0004	_	4.38 ± 1.42	3490	_

[a] EC_{50}: concentration of compound required to achieve 50% protection of MT-4 cell cultures against HIV-1-induced cytotoxicity, as determined by the MTT method. [b] CC_{50}: concentration required to reduce the viability of mock-infected cell cultures by 50%, as determined by the MTT method. [c] SI: selectivity index, the ratio of CC_{50}/EC_{50}. [d] CV: cyanovinyl. [e] X1: ≥1 or <1. [f] Used for comparison. The data were obtained from the same laboratory with the same method (Prof. Christophe Pannecouque, Rega Institute for Medical Research, KU Leuven, Belgium).[13] [g] ND: not determined. [h] Used for comparison. The data were obtained from the same laboratory with the same method (Prof. Christophe Pannecouque, Rega Institute for Medical Research, KU Leuven, Belgium).[21]

DOI: 10.1021/acs.jmedchem.8b01729
J. Med. Chem. 2019, 62, 2083−2098

Table 2. Antiviral Activity against Several HIV-1 Mutant Strains in MT-4 Cells

	EC_{50} (μM)[a]					
compds	E138K	L100I	K103N	Y181C	Y188L	F227L + V106A
10c	0.14 ± 0.037	0.41 ± 0.030	0.068 ± 0.016	0.91 ± 0.069	4.93 ± 0.0099	1.80 ± 0.19
10d	0.089 ± 0.0023	0.11 ± 0.073	0.23 ± 0.20	0.47 ± 0.088	>5.22	1.03 ± 0.13
10e	0.38 ± 0.029	0.70 ± 0.14	0.46 ± 0.017	2.60 ± 0.37	≥7.80	3.23 ± 1.40
10f	0.45 ± 0.070	2.15 ± 1.76	0.50 ± 0.071	6.54 ± 0.76	>6.97	≥6.82
11a	0.13 ± 0.015	0.20 ± 0.053	0.020 ± 0.0095	0.42 ± 0.0069	>4.03	0.15 ± 0.032
11b	0.15 ± 0.032	0.28 ± 0.13	0.068 ± 0.0050	0.57 ± 0.044	>4.27	≥1.14
11c	0.0075 ± 0.0016	0.010 ± 0.0041	0.0036 ± 0.00014	0.025 ± 0.0031	1.62 ± 0.24	0.11 ± 0.025
11d	0.036 ± 0.0040	0.13 ± 0.0090	0.025 ± 0.0046	0.33 ± 0.045	8.35 ± 0.52	0.47 ± 0.011
AZT	0.014 ± 0.0071	0.0036 ± 0.00026	0.011 ± 0.0019	0.0056 ± 0.0016	0.0051 ± 0.0013	0.0062 ± 0.0013
NVP	0.16 ± 0.087	1.64 ± 0.47	10.9 ± 1.53	>15.0	>15.0	>15.0
EFV	0.0060 ± 0.00045	0.052 ± 0.000	0.089 ± 0.019	0.0060 ± 0.0018	0.24 ± 0.046	0.27 ± 0.027
ETR	0.015 ± 0.0049	0.0074 ± 0.00065	0.0039 ± 0.00032	0.021 ± 0.0047	0.027 ± 0.0054	0.026 ± 0.0026

[a] EC_{50}: concentration of compound required to achieve 50% protection of MT-4 cell cultures against HIV-1-induced cytotoxicity, as determined by the MTT method.

antiviral evaluation results, interpreted as EC_{50} (anti-HIV potency), CC_{50} (cytotoxicity), and SI (selectivity index, CC_{50}/EC_{50} ratio), are summarized in Tables 1 and 2.

All compounds exhibited moderate to excellent potency against WT HIV-1 strain with EC_{50} values ranging from 0.20 to 0.0035 μM, which were superior to the reference drugs 3TC (EC_{50} = 6.41 μM) and NVP (EC_{50} = 0.24 μM), as well as the previously reported compound **WC-II-4b** (EC_{50} = 0.93 μM). Among them, **11c** turned out to be the most active inhibitor with an EC_{50} value of 0.0035 μM, which was much more lower than those of 3TC and NVP, 3-fold lower than that of AZT (EC_{50} = 0.011 μM), and equivalent to that of ETR. As expected, none of the target compounds exhibited inhibitory activity against the HIV-2 strain at subtoxic concentrations (data were not shown in this article).

Moreover, compound **11c** showed activity against the K103N/Y181C double mutant HIV-1 strain (RES056) at a submicromolar concentration (EC_{50} = 0.79 μM), which was more active than the reference drug NVP (EC_{50} > 15.0 μM) and the precursor compound **WC-II-4b** (EC_{50} > 6.9 μM), though still less potent than AZT, EFV, and ETR.

Table 2 shows that these selected compounds with potent activity against WT HIV-1 strain also demonstrated moderate to prominent activity against the mutant HIV-1 strains. Among them, **11c** demonstrated the most excellent activity against HIV-1 single mutations E138K and K103N with EC_{50} values as 0.0075 and 0.0036 μM, respectively. The antiviral potency against these HIV-1 variants are summarized as follows:

(1) In case of the E138K mutant strain which is the key drug-resistant HIV-1 strain to DAPYs, three compounds **10d**, **11c**, and **11d** exhibited potent activity at two- or single-digit nanomolar concentrations, and the others showed inhibitory activity at submicromolar concentrations. To our delight, **11c** was 2 times more potent than ETR (EC_{50} = 0.015 μM).

(2) For K103N, that is the most prevalent single mutant strain, **10c** and **11a**−**d** displayed low EC_{50} values ranging from 0.068 to 0.0036 μM, being more potent than EFV (EC_{50} = 0.089 μM). Again, **11c** possessed slightly improved activity than that of ETR (EC_{50} = 0.0039 μM).

(3) As for the other two single-mutant strains, L100I and Y181C, it was noted that only compound **11c** exhibited EC_{50} values at nanomolar levels (EC_{50} = 0.010 and 0.025 μM, respectively), which were both mildly higher than those of ETR (EC_{50} = 0.0074 and 0.021 μM, respectively). **11c** was much more active against L100I variant than EFV (EC_{50} = 0.052 μM) while less potent against Y181C mutant strain than EFV (EC_{50} = 0.0060 μM).

(4) All of the selected compounds showed moderate or lost activity against Y188L and F227L + V106A mutant strains.

Based on the biological evaluation results (Table 1), preliminary SARs were investigated:

The contribution of R_1 substituents of these new DAPY-typed derivatives to the anti-HIV activities was first assessed. Through pairwise comparison on potency, namely, **10a** (EC_{50} = 0.20 μM) and **11b** (EC_{50} = 0.026 μM), **10d** (EC_{50} = 0.0072 μM) and **11c** (EC_{50} = 0.0035 μM), and **10e** (EC_{50} = 0.055 μM) and **11d** (EC_{50} = 0.0069 μM), it could be concluded that the cyanovinyl group was more favorable for activity than the cyano group. Next, we focused our attention on the fragments introduced into the tolerant region I. It was obvious that this region was indeed highly tolerated by various substituents. Also, the size of the chemical groups connected to the terminal of piperazine/piperidine was a major determinant for the anti-HIV-1 activity, which is illustrated in Table 1. Smaller and hydrophilic groups, such as methylsulfonyl and sulfamide, were favorable to the activity against WT HIV-1 strain (**10e**, **10f** vs **10a**, **11c** vs **11a**, **11d** vs **11b**). In addition, compound **17** exhibited anti-HIV-1 (III_B) potency at a submicromolar concentration, though inferior to most compounds in **10a**−**f** subseries, indicating that the triazine ring was an alternative core for DAPY-typed derivatives.

Moreover, it is noteworthy that the morpholine-bearing compound **10c** had a CC_{50} value of 23.0 μM, demonstrating a relative lower cytotoxicity. Most importantly, compound **11c** was found to possess the lowest cytotoxicity (CC_{50} ≥ 173 μM), which was much lower than that of RPV (CC_{50} = 4.38 μM)[21] and thus had a high SI (SI ≥ 48 774). As it has been extensively reported that the cyanovinyl containing HIV-1 NNRTIs including RPV possess high cytotoxicity in MT-4 cells, compound **11c** featuring a cyanovinyl function group was truly an interesting molecule.

In general, these biological results demonstrated that introducing hydrophilic and polar functional groups, including

DOI: 10.1021/acs.jmedchem.8b01729
J. Med. Chem. 2019, 62, 2083−2098

morpholine or methylsulfonyl and sulfamide-substituted piperazine/piperidines, into the right wing of DAPYs to target the tolerant region I was acceptable and may improve antiviral potency, especially to the E138K and K103N mutant HIV-1 strains.

In order to confirm the mode of action of these newly synthesized DAPY-typed derivatives, we further tested all the compounds for their ability to inhibit recombinant WT HIV-1 RT, with NVP, EFV, and RPV as reference drugs (Table 3).

Table 3. Inhibitory Activity of the New Compounds against HIV-1 RT (WT)

compds	EC_{50} (μM)[a]	IC_{50} (μM)[b]	pEC_{50}[c]	pIC_{50}[d]
10a	0.20 ± 0.019	0.413 ± 0.012	6.70	6.38
10b	0.19 ± 0.011	0.277 ± 0.001	6.72	6.56
10c	0.011 ± 0.0015	0.042 ± 0.002	7.96	7.38
10d	0.0072 ± 0.0029	0.049 ± 0.000	8.14	7.31
10e	0.055 ± 0.014	0.079 ± 0.011	7.26	7.10
10f	0.092 ± 0.045	0.152 ± 0.011	7.04	6.82
11a	0.015 ± 0.0088	0.297 ± 0.041	7.82	6.53
11b	0.026 ± 0.017	0.499 ± 0.025	7.59	6.30
11c	0.0035 ± 0.00075	0.067 ± 0.030	8.46	7.17
11d	0.0069 ± 0.0015	0.076 ± 0.023	8.16	7.12
17	0.12 ± 0.034	0.442 ± 0.138	6.92	6.35
NVP	0.24 ± 0.024	0.595 ± 0.146	6.62	6.23
EFV	0.0013 ± 0.00032	0.007 ± 0.003	8.89	8.15
RPV	0.0013 ± 0.0004[e]	0.022 ± 0.004	8.89	7.66
ETR	0.0035 ± 0.00018	0.011 ± 0.000[f]	8.46	7.96

[a]EC_{50}: the anti-HIV-1 (III_B) activity in MT-4 cells, as indicated in the Table 1. [b]IC_{50}: the RT inhibition assay is performed with the EnzChek Reverse Transcriptase Assay kit (Molecular Probes, Invitrogen). [c]pEC_{50}: −log EC_{50}. [d]pIC_{50}: −log IC_{50}. [e]Used for comparison. The data were obtained from the same laboratory with the same method (Prof. Christophe Pannecouque, Rega Institute for Medical Research, KU Leuven, Belgium).[21] [f]Used for comparison. The data were obtained from the same laboratory with the same method (Prof. Christophe Pannecouque, Rega Institute for Medical Research, KU Leuven, Belgium).[13]

These compounds displayed HIV-1 RT inhibitory activity in the range of 0.499−0.042 μM. Compound **10c** exhibited the most active RT inhibitory activity with an IC_{50} value (0.042 μM) in the same magnitude with the reference drug RPV (0.022 μM). Overall, there was a close correlation between the anti-HIV-1 (III_B) activity (EC_{50}) and the RT inhibitory activity (IC_{50}) of these compounds. This was shown in a linear regression curve with both biological results for all new compounds in Tables 1 and 3, including the reference drugs NVP and EFV (Figure 3). The results demonstrated that these inhibitors exhibited antiviral activity by inhibiting the RT enzyme and could act as typical HIV-1 NNRTIs.

Docking and Molecular Dynamics Simulation Studies. To better elucidate the anti-HIV potency of these new DAPY derivatives at a molecular level and to further understand the structural basis of their binding modes in the NNIBP, a molecular modeling study of a subset of representative compounds (**11c**, **10c**, and **10a**) together with the lead compound ETR was performed using docking and molecular dynamics (MD) calculations.

The crystallographic structure (PDB code: 3M8Q)[23] of HIV-1 RT in complex with the NNRTI 3,5-dimethyl-4-{[2-({1-[4-(methylsulfonyl)benzyl]piperidin-4-yl}amino)pyrimidin-4-yl]-oxy}benzonitrile (DJZ; Supporting Information Table S1 and

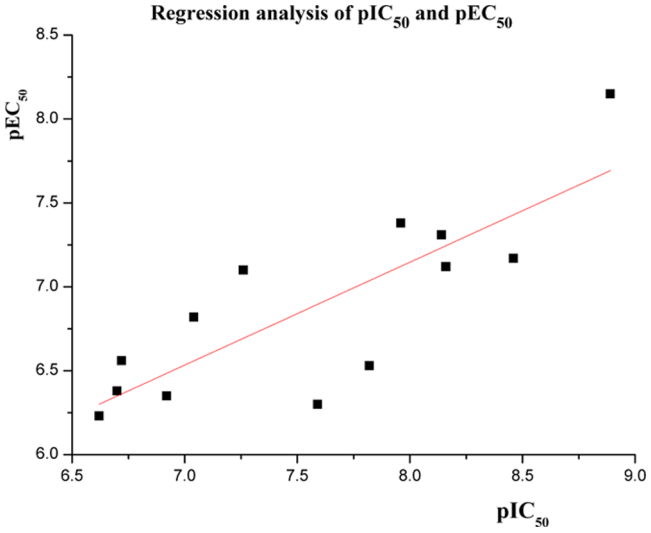

Figure 3. Regression analysis of pIC_{50} and pEC_{50} values for the newly synthesized DAPY-typed derivatives.

Figure S1) was used to perform a "core-constrained" flexible docking of ligands in the WT enzyme. Additional docking calculations were performed for the E138K and K103N variants of the HIV-1 RT, which were built up by replacing E138 and K103 in 3M8Q by Lys and Asn, respectively, taking into account the proper arrangement of the side chains as found upon inspection of the X-ray structures 2HNY and 3MED, which correspond to the complexes of NVP and ETR with the E138K and K103N mutated HIV-1 RT, respectively. Finally, the potential influence of the structural water molecule (567), which mediates the interaction of the protonated piperidine nitrogen of DJZ with residues K103 and P236 in 3M8Q, was also examined.

Docking calculations performed for DJZ and ETR led to poses that reproduced the crystallographic binding mode [root-mean square deviation (rmsd) of the ligand <0.1 Å; Supporting Information Figures S1 and S2], irrespective of the introduction of the mutations at positions 138 and 103 as well as of the presence of the structural water 567 (Supporting Information Table S2), as noted in similar scores obtained for each ligand in the 6 protein models (3M8Q, $3M8Q_{E138K}$, and $3M8Q_{K103N}$, with and without water 567), generally being comprised between −10.0 and −12.5 kcal/mol. This finding can be attributed to the large structural resemblance found in the NNRTI binding site for structures 3M8Q, 3MED, and 2HNY (Supporting Information Figure S1). The binding modes predicted for ligands **11c**, **10c**, and **10a** were also consistent with the arrangement of DJZ and ETR, although the most notable trait was the identification of two orientations of the piperazine (**11c**), morpholine (**10c**), and piperidine (**10a**) ring in the tolerant region I of the NNRTI binding site (Supporting Information Table S3 and Figure S3). In one of these arrangements, the protonated nitrogen is pointing toward the backbone carbonyl groups of His235 and Pro236, and in the other the terminal ring is rotated by almost 180° (denoted *reversed* hereafter).

The analysis of the MD simulations revealed that the ligand−protein complexes were stable in all cases, as noted in the comparison of the time evolution of the rmsd profiles determined for the residues that shape the NNRTI binding site (taken as the set of residues located at 5 Å from the ligand in

DOI: 10.1021/acs.jmedchem.8b01729
J. Med. Chem. 2019, 62, 2083−2098

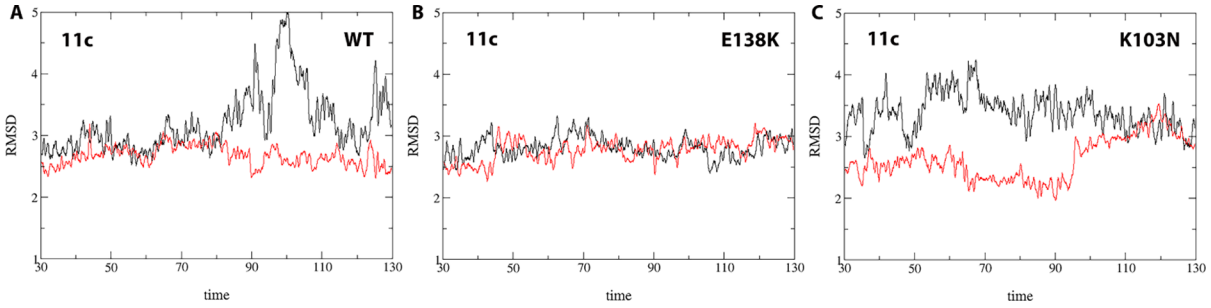

Figure 4. Time (ns) evolution of the rmsd (Å) profile determined for the complexes between **11c** with (A) WT 3M8Q, (B) 3M8Q$_{E138K}$, and (C) 3M8Q$_{K103N}$. The rmsd profile determined for the whole protein backbone is shown in black, and for the heavy atoms of the binding site and ligand in red.

the energy-minimized complex) and the ligand, the rmsd being, on average, generally close to 2.7 Å (Figure 4 for complexes with **11c**; see also Supporting Information Figure S4 for complexes with **10c** and ETR).

Compound **11c** adopted a binding orientation characterized by the classical "U" shape conformation in the NNIBP similar to that of ETR (Figure 5A). Distinct traits characterize the binding mode of **11c** in the NNIBP binding site. The 2,6-dimethyl-4-cyanovinylphenoxy moiety filled a hydrophobic subpocket composed by the aromatic side chains of Tyr181, Tyr188, and Trp229, resulting in potential van der Waals (vdW) interactions with the aromatic side chains of these residues. Furthermore, the

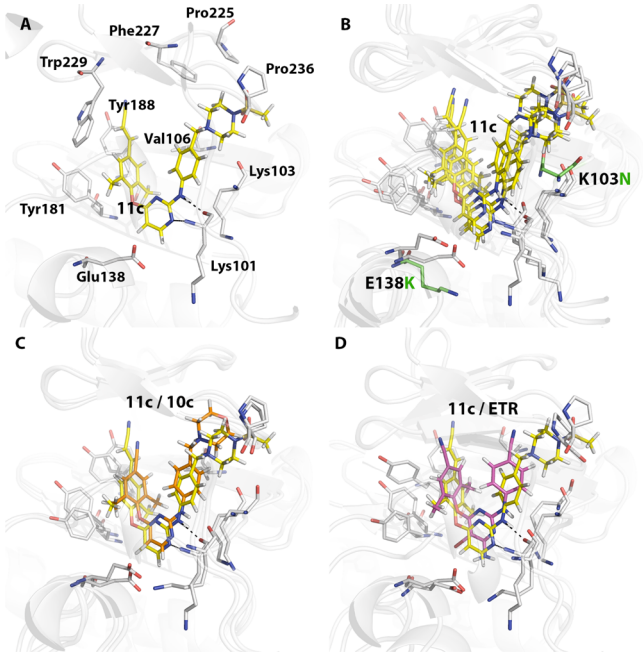

Figure 5. (A) Binding mode of **11c** in NNIBP of WT HIV-1 RT (PDB code: 3M8Q). (B) Superposition of the binding mode of **11c** in NNIBP of WT 3M8Q, 3M8Q$_{E138K}$ and 3M8Q$_{K103N}$. (C) Superposition of the binding mode of **11c** and **10c** in NNIBP of WT 3M8Q. (D) Superposition of the binding mode of **11c** and **ETR** in NNIBP of WT 3M8Q. The protein backbone is shown as gray carton, and selected residues are highlighted as sticks (mutations of Glu138 and Lys103 to Lys and Asn, respectively, are shown as sticks with green-colored carbon atoms; hydrogen atoms are omitted for the sake of clarity). Ligands are shown as sticks with carbon atoms colored in yellow (**11c**), orange (**10c**), and magenta (ETR). Hydrogen bonds are indicated as dashed black lines (red).

1′-N of the pyrimidine ring and the NH linker of the compound formed dual hydrogen bonds with the backbone carbonyl oxygen and amide NH groups of Lys101, which appear to be crucial for the binding of the ligand. Thus, the interaction NH···O$_{K101}$ was very stable along the trajectory with WT 3M8Q, as noted in an average distance of 2.93 ± 0.04 Å along the last 100 ns of the MD simulation, whereas the interaction 1′-N···HN$_{K101}$ resulted to be a weaker hydrogen bond (average distance of 3.62 ± 0.30 Å). Finally, the methylsulfonyl piperazine motif located in the tolerant region I was exposed at the protein/solvent interface, with the piperazine ring being stacked against Pro236 (in the *reversed* arrangement), and the methylsulfonyl group being located close to Pro225 and Phe227, or adopting an alternative arrangement that enables a transient hydrogen-bond interaction with the backbone of Val106.

The binding mode of **11c** to the WT 3M8Q and to the 3M8Q$_{E138K}$ and 3M8Q$_{K103N}$ variants was highly similar, as noted in the superposition of the final snapshots collected at the end of the MD simulations for these systems (Figure 5B). The results confirm the relevant contribution of the NH···O$_{K101}$ interaction (average distance of 2.94 ± 0.04 Å), which is supplemented by the weaker 1′-N···HN$_{K101}$ hydrogen bond (average distance of 3.50 ± 0.19, and 3.83 ± 0.31 Å), the occupancy of the subpocket formed by Tyr181, Tyr188, and Trp229, and the flexibility of the methylsulfonyl piperazine motif in the tolerant region I, including the conformational change of the protonated piperazine ring to the *reversed* arrangement along the trajectory run for the **11c**−3M8Q$_{E138K}$ complex.

To further check the preservation of the features that mediate the binding mode of **11c**, two MD simulations were also run for compound **10c** bound to WT 3M8Q, differing in the orientation of the morpholine ring. The two structures converged to a similar binding mode (Supporting Information Figure S5), which also matched the arrangement of **11c** (Figure 5C), where the morpholine ring adopted the *reversed* arrangement, being stacked against Pro236. On the other hand, the binding of the central pyrimidine ring was assisted by the two hydrogen bonds mentioned above (average distances of 2.93 ± 0.05 and 3.57 ± 0.26 Å for the NH···O$_{K101}$ and 1′-N···HN$_{K101}$ interactions, respectively).

As a final remark, let us note that ETR also adopted a stable binding mode in the WT 3M8Q and the two mutated variants (Supporting Information Figure S6), which matches well the binding of **11c** (Figure 5D). The NH···O$_{K101}$ and 1′-N···HN$_{K101}$ interactions were maintained along the trajectory in all cases, as noted in average distances of 2.89−2.94 and 3.40−3.76 Å, respectively, in the three MD simulations. However, it is worth noting that the binding is further assisted by an additional

DOI: 10.1021/acs.jmedchem.8b01729
J. Med. Chem. 2019, 62, 2083−2098

Table 4. Water Solubility, tPSA, clog *P*, LE, and LLE Values of Compounds 10c, 10d, 11c, 11d, and ETR

compds	10c	10d	11c	11d	ETR
water solubility (pH = 7) (μg/mL)	33.40 ± 0.04		30.92 ± 0.02		≪1[27]
tPSA[a] (<140 Å^2)	83.31	111.45	111.45	120.24	120.65
clog *P*[a] (<5)	4.36	3.78	4.54	4.82	5.03
LE[b] (>0.3)	0.35	0.32	0.31	0.29	0.41
LEE[c] (>5)	3.60	4.36	3.92	3.34	3.43

[a]tPSA and clog *P*: calculated by free online software (http://www.molinspiration.com/). tPSA, topological polar surface area. [b]LE: calculated by the formula $-\Delta G/N_{(\text{non-hydrogen atom})}$, where standard free energy change $\Delta G = -RT \ln Kd$, presuming $Kd \approx EC_{50}$; negative logarithm values of potency (pEC_{50}) converted from experimental data against WT HIV-1 III_B. *R* is the gas constant, and *T* is 300 K. $N_{(\text{non-hydrogen atom})}$ is the number of non-hydrogen atoms. [c]LEE: calculated by the formula pEC_{50} − clog *P*.

Table 5. Inhibitory Activity on CYP2C9, CYP2C19, CYP2D6, CYP3A4M, and CYP3A4T of Compound 11c and Positive Controls

CYP subtypes	selective inhibitors	inhibitory activity (IC_{50}, μM)	compd	inhibitory activity (IC_{50}, μM)
CYP2C9	sulfaphenazole	0.847	**11c**	22.3
CYP2C19	(+)-*N*-3-benzylnirvanol	0.124	**11c**	27.0
CYP2D6	quinidine	0.263	**11c**	>50
CYP3A4M	ketoconazole	0.0183	**11c**	20.5
CYP3A4T	ketoconazole	0.0563	**11c**	7.82

hydrogen bond formed between ETR and the carboxylate group of Glu138. Overall, the binding conformation of **11c** revealed a remarkable superposition to that of ETR, giving rise to its potent anti-HIV and RT inhibition activities.

Taken together, these findings provide a basis to justify that **11c** possessed good activity against the key drug resistant variant E138K to the DAPY-typed HIV-1 NNRTIs. Furthermore, keeping in mind the flexibility of the tolerant region I, it can be speculated that the detrimental effect due to the introduction of the Boc group on the inhibitory activity (compare **11a** and **11b** with regard to **11c**, and **10a** and **10b** relative to **10c**) may result from the steric hindrance that impedes an appropriate "closure" of the loops that shape this region. In turn, this would prevent a proper packing of the ligand with the surrounding residues, while it would facilitate the access of water molecules that may promote release of the ligand from the binding pocket. Overall, present results confirmed our rational drug design as an effective strategy to overcome the drug-resistance issues.

Water Solubility and Other Drug-Like Properties. To validate our hypothesis, we performed water solubility measurement of the representative compounds **10c** and **11c**. As revealed in Table 5, both compounds possessed significantly improved water solubility than that of ETR. Besides, it should be noted that the morpholine-bearing compound **10c** had the best water solubility of 33.4 μg/mL. Coincidentally, in lead optimization programs in medicinal chemistry, the morpholine was commonly introduced into solvent exposed areas as a privileged solubilizing group to improve solubility or pharmacokinetic properties of a prospective drug scaffold, exemplified by the approved drugs copanlisib and gefitinib, as well as many bioactive compounds with greatly improved solubility[24] (including our previously reported compound **WC-II-4b**). Additionally, polar surface area (PSA, a very useful prediction parameter of oral bioavailability) of four representative compounds **10c**, **10d**, **11c**, and **11d** as well as of ETR was calculated using free online software (http://www.molinspiration.com/), and the results are also shown in Table 5. It is suggested that drugs with a PSA <60 Å^2 are almost completely (more than 90%) absorbed, whereas drugs with a PSA >140 Å^2 are absorbed to less than 10%.[25,26] Compared with that of ETR, the PSA values of these new derivatives indicated that our modifications at the right portion of ETR could possibly increase the oral bioavailability.

In recent years, ligand efficiency (LE, $-\Delta G/N_{(\text{non-hydrogen atom})}$) and ligand-lipophilicity efficiency (LLE, pEC_{50} − clog *P*) which combine both "potency and lipophilicity" have emerged as important metrics in many drug discovery programs, usefully directing hit and lead optimization. Desirable leads commonly exhibit LE > 0.3, LLE >5 or greater, and clog *P* <5. We therefore calculated the metrics of these four compounds together with ETR (Table 4). Fortunately, all of the selected compounds met acceptable levels for LE and clog *P*. The LLE indices of three compounds **10c**, **10d**, and **11c** were better than that of ETR. Certainly, they still needed to be improved to satisfy the standard level.

In Vitro Effects of 11c on CYP Enzymatic Inhibitory Activity. As is well known, metabolizing enzymes in the liver (e.g. cytochrome P450, CYP) are responsible for the majority of drug metabolism in vivo. Among them, CYP3A, CYP2D6, and CYP2C subtypes are involved in metabolism of about 90% of the marketed drugs.[28] Drugs can also interact with the CYP enzymes, by inhibiting their enzymatic activity (CYP inhibition) and/or through activating nuclear receptors which leads to induction of their gene expression (CYP induction). Therefore, metabolism-mediated drug−drug interactions (DDI) may occur when co-administrating different drugs, leading to decreased therapeutic effect or adverse reaction profile. According to disclosed information, ETR is an inducer of CYP3A4 and inhibitor of CYP2C9 and CYP2C19, and it can result in many DDI when co-administrated with other anti-HIV-1 drugs such as integrase strand inhibitors, protease inhibitors, CCR5 antagonists, and so on, which limits the selection of concomitant antiretrovirals. We performed the study of inhibitory activity of compound **11c** on main CYP drug metabolizing enzymes, with selective inhibitors of these enzymes as positive controls. The results in Table 5 indicated that **11c** displayed no significant CYP enzymatic inhibition of CYP2C9, CYP2C19, CYP2D6, CYP3A4M, and CYP3A4T (if one compound inhibits CYP enzymes with IC_{50} < 3 μM, it is regarded as a potent CYP enzyme inhibitor[29]), which preliminarily proved that our

DOI: 10.1021/acs.jmedchem.8b01729
J. Med. Chem. 2019, 62, 2083−2098

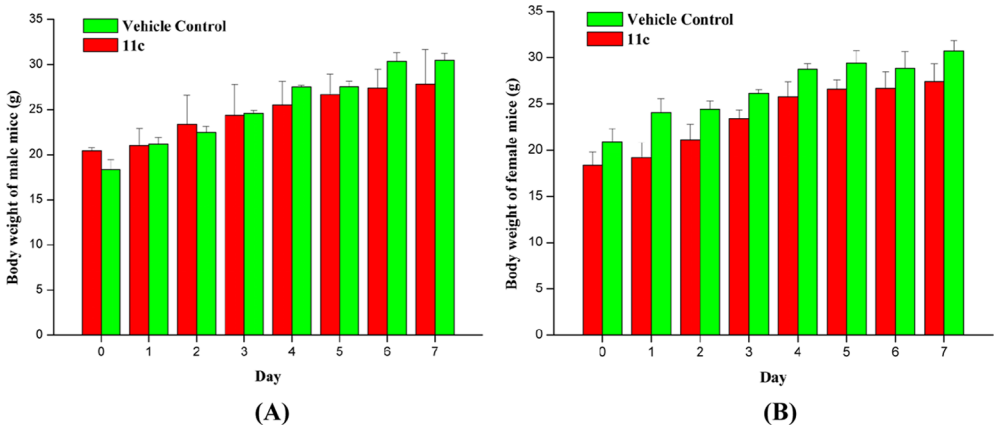

Figure 6. (A) Body weight of male mice (g)-time (day); (B) body weight of female mice (g)-time (day).

compound **11c** had less potential to induce side effects in the liver and DDI.

Acute Toxicity Assessment of 11c in Healthy Mice. Single-dose acute toxicity of **11c** in healthy mice was studied regarding to its relatively low cytotoxicity. After intragastric administration of **11c** at a dose of 2000 mg·kg^{-1}, no mice died, and there was no abnormality of their behaviors (lethargy, clonic convulsion, anorexia, and ruffled fur). All mice in drug-administration groups grew normally the same as the mice in control groups. On the whole, the body weights of both male and female mice increased gradually over the 1 week period (Figure 6), and there was no obvious difference in the weight gain. Therefore, **11c** was well-tolerated at a dose of 2000 mg·kg^{-1} with no acute toxicity.

Subacute Toxicity Assessment of 11c in Healthy Mice. For assessing the in vivo safety of **11c**, we further investigated its subacute toxicity in healthy mice. The mice in test groups were po administered with a dose of 50 mg·kg^{-1} of **11c** every second day for 14 days. Again, no mice died, and no abnormality of their behaviors (lethargy, clonic convulsion, anorexia, and ruffled fur) and body weight increase were observed during the treatment period. The body weight of both males and females in test groups increased gradually and they grew normally the same as the control groups (Figure 7). Additionally, the five most important organs (heart, liver, spleen, lungs, and kidneys) were examined by hematoxylin−eosin (HE) staining after dissecting all of the mice, and it was observed that no marked pathological damage occurred after treatment with **11c** (Figure 8). The subacute toxicity evaluation results indicated that **11c** possessed favorable in vivo safety profiles.

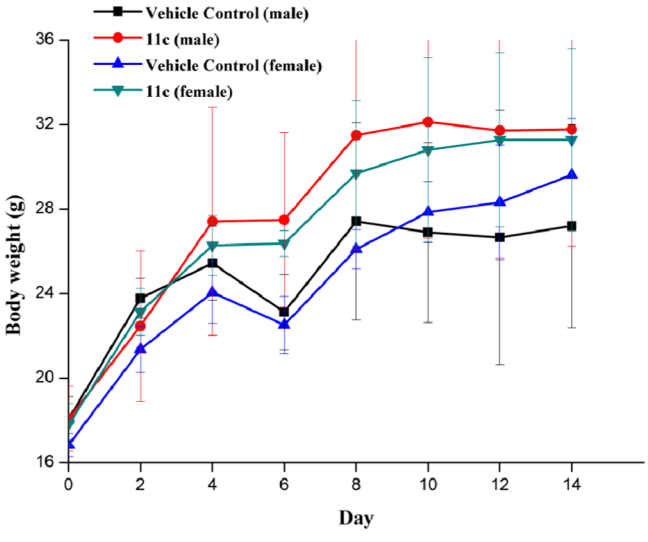

Figure 7. Body weight of all mice in four groups (g)-time (day).

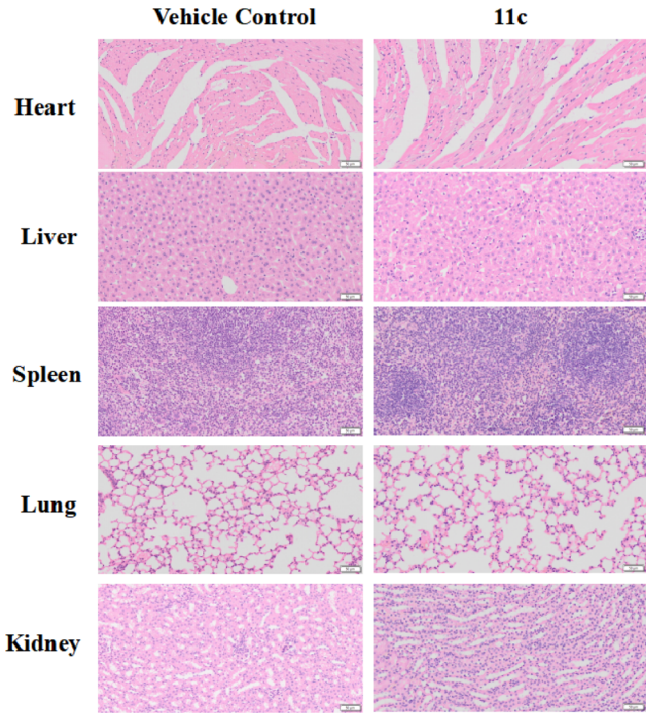

Figure 8. HE staining results of five organs of healthy mice treated with **11c** or vehicle solution after 14 days. Scale bars represent 50 μm.

CONCLUSIONS

In summary, we have designed and synthesized a novel series of DAPY-typed HIV-1 NNRTIs targeting the tolerant region I of NNIBP, with hydrophilic morpholine or methylsulfonyl and sulfamide-substituted piperazine/piperidines being introduced into the right wing of DAPYs. The anti-HIV-1 assay results showed that all compounds exhibited moderate to excellent potency against WT HIV-1 strain. The most active inhibitor **11c** (EC_{50} = 0.0035 μM) was as potent as the lead compound ETR, with a prominent safety index higher than 48 774. Moreover, it

DOI: 10.1021/acs.jmedchem.8b01729
J. Med. Chem. 2019, 62, 2083−2098

displayed fairly potent activity against the most frequently emerged K103N/Y181C double mutant HIV-1 strain (EC_{50} = 0.79 μM). Most importantly, compound **11c** displayed prominent activity against the E138K mutant virus (EC_{50} = 0.0075 μM) that is a key drug-resistant variant to DAPYs, which is 2-fold better than that of ETR, and also exhibited a slightly improved potency against K103N mutant strain (EC_{50} = 0.0036 μM) over that of ETR (EC_{50} = 0.0039 μM). The HIV-1 RT inhibition assay preliminarily confirmed the binding target. Besides, molecular simulation studies provided key clues for the remarkable anti-HIV activity of these new inhibitors.

Further test showed a dramatic improvement in the solubility of two representative compounds **10c** and **11c** comparing to that of ETR, which validated our hypothesis well. Compound **11c** also exhibited favorable LE and LLE values. In addition, **11c** displayed no significant inhibition on main CYP enzymes. Lastly but most importantly, compound **11c** showed no acute toxicity at a dose of 2000 mg·kg^{-1} and also no subacute toxicity at a dose of 50 mg·kg^{-1} in healthy mice. Combined with the in vitro low cytotoxicity and CYP inhibition results, it was indicated that **11c** possessed favorable safety profiles. Taken together, we consider that **11c** is a promising lead for further structural optimization.

EXPERIMENTAL SECTION

Chemistry. All melting points (mp) were determined on a micromelting point apparatus and are uncorrected. Mass spectra were performed on an LC autosampler device: Standard G1313A instrument by electrospray ionization. ^{1}H NMR and ^{13}C NMR spectra were obtained on a Bruker AV-400 spectrometer (Bruker BioSpin, Fällanden, Switzerland) in the indicated solvent DMSO-d_6. Chemical shifts were expressed in δ units (ppm), using TMS as an internal standard, and J values were reported in hertz (Hz). Thin-layer chromatography (TLC) was performed on silica gel GF254. Spots were visualized with iodine vapor and/or by irradiation with UV light (λ 254 nm). Flash column chromatography was carried out on columns packed with silica gel 60 (200−300 mesh). Solvents were of reagent grade and, if needed, were purified and dried by standard methods. The key reagents were purchased from commercial suppliers and with no further purification when used. Rotary evaporators were served in concentration of the reaction solutions under reduced pressure. Analysis of the sample purity was performed on a Waters e2695 HPLC system using a Waters 2998 detector and GOLD-C18 analytical column (5 μm; 250 mm × 4.6 mm). High performance liquid chromatography (HPLC) eluent conditions: acetonitrile/water, varied as follows: from 0 to 15 min, acetonitrile increased from 40 to 90% gradiently; from 15 to 16 min, acetonitrile decreased from 90 to 40% gradiently; from 16 to 18 min, acetonitrile was kept at 40%. Flow rate, 1.0 mL/min; UV detection, from 200 to 600 nm; temperature, ambient; injection volume, 2 μL. The purity of representative final compounds was checked by HPLC and all was >95%.

Preparation of Intermediates 5a−d. *tert-Butyl(1-(4-aminobenzyl)piperidin-4-yl)carbamate (**5a**).* To a solution of 4-nitrobenzyl bromide **3** (2.16 g, 0.01 mol) and 4-*N*-Boc-aminopiperidine (2.00 g, 0.01 mol) in dichloromethane (20 mL), triethylamine (1.21 g, 0.012 mol) was added. The resulting mixture was stirred at room temperature (rt) until completion monitored by TLC. The reaction mixture was washed with water and then saturated brine. The organic layer was separated, dried over anhydrous Na_2SO_4, filtered, and concentrated under reduced pressure. The residue was recrystallized using ethyl acetate/petroleum ether to afford *tert*-butyl(1-(4-nitrobenzyl)piperidin-4-yl)carbamate (**4a**) as a white solid. Then, intermediate **4a** (1.0 equiv) was dissolved in 20 mL anhydrous methanol and then stannous chloride dihydrate (5.0 equiv) was added. The reaction mixture was stirred at rt under a nitrogen atmosphere. NaOH (aq; 2% w/w) was added into the mixture to adjust pH to 7. The resulting white solid was filtered off and washed by ethyl acetate. The filtrate was added saturated brine and ethyl acetate. The combined organic layers were dried over anhydrous Na_2SO_4, filtered, concentrated under reduced pressure, and dried in vacuum to finally afford intermediate **5a** as a white solid. The crude intermediate **5a** was used in next step without further purification.

For intermediates **5b−d**, the synthetic procedures were the same as for **5a**, but the starting materials were 4-amino-1-Boc-piperidine, morpholine, and 1-Boc-piperazine, respectively.

Preparation of Compound 7. *tert-Butyl(chlorosulfonyl)-carbamate (**7**).* Chlorosulfonyl isocyanate **6** (0.17 g, 1.2 mmol) and *t*-BuOH (0.089 g, 1.2 mmol) were dissolved in dichloromethane (5 mL), and then the resulting mixture was stirred at 0 °C until completion. After standing for some hours, the precipitated solid was filtered, washed with *n*-hexane, and dried to provide intermediate **7** (*tert*-butyl(chlorosulfonyl)carbamate) as a colorless solid. Yield: 81%.

Preparation of Compounds 9a and 9b. *4-((2-Chloropyrimidin-4-yl)oxy)-3,5-dimethylbenzonitrile (**9a**).* To a solution of 4-hydroxy-3,5-dimethylbenzonitrile (1.47 g, 0.01 mol) and potassium carbonate (1.66 g, 0.012 mol) in dimethylformamide (DMF) (20 mL), 2,4-dichloropyrimidine **8** (1.49 g, 0.01 mol) was added, and the mixture was stirred at 50 °C for 4 h until completion. Water (200 mL) was added, and the mixture was extracted with EtOAc (3 × 50 mL). The combined organic layers were washed with saturated brine, dried over anhydrous Na_2SO_4, filtered and concentrated under reduced pressure, and finally recrystallized using EtOAc and petroleum ether to provide the pure intermediate **9a**. White solid. Yield: 82%. mp 194.6−196.0 °C. ESI-MS m/z: 260.3 $(M + 1)^+$, 262.3 $(M + 3)^+$, $C_{13}H_{10}ClN_3O$, (259.05).

*(E)-3-(4-((2-Chloropyrimidin-4-yl)oxy)-3,5-dimethylphenyl)-acrylonitrile (**9b**).* The synthetic method was similar to that described for **9a**, except that the starting material (*E*)-3-(4-hydroxy-3,5-dimethylphenyl)acrylonitrile (1.73 g, 0.01 mol) reacted with 2,4-dichloropyrimidine **8** (1.49 g, 0.01 mol). White solid. Yield: 78%. mp 119.1−120.2 °C. ESI-MS m/z: 286.3 $(M + 1)^+$, 288.3 $(M + 3)^+$, 303.5 $(M + 18)^+$, $C_{15}H_{12}ClN_3O$, (285.07).

*General Procedure for the Preparation of Target Compounds **10a−c** and **11a, 11b**.* A mixture of the intermediates **9a** or **9b** (1.0 mmol), well-prepared intermediates **5a−d** (1.0 mmol), $Pd(OAc)_2$ (0.05 mmol), xantphos (0.05 mmol), and Cs_2CO_3 (1.5 mmol) was dissolved in 1,4-dioxane (10 mL), and then the solution was heated at 90 °C for 12 h under an N_2 atmosphere. After cooling to rt, the mixture was filtered and concentrated under reduced pressure. Finally, the residue was further purified by silica gel chromatography with methanol/dichloromethane as eluent and recrystallized from methanol to give some target compounds **10a−c** and **11a**, **11b**.

*General Procedure for the Preparation of Target Compounds **10d−f** and **11c, 11d**.* The Boc-containing target compound **10a** was dissolved in dichloromethane/trifluoroacetic acid (v/v, 1/1), and the reaction mixture was stirred at rt until completion monitored by TLC. After removal of the excess solvent under reduced pressure, saturated potassium carbonate aqueous solution was added. After extraction with dichloromethane, the combined organic phase was washed with saturated brine, dried over anhydrous Na_2SO_4, filtered, and concentrated under reduced pressure. Then, the residue was further purified by silica gel chromatography with methanol/dichloromethane as eluent to afford the key intermediate **12a**. The synthetic method for the preparation of **12b−d** was similar to that described for **12a**, except that the starting materials were the rest Boc-containing target compounds **10b**, **11a**, and **11b** respectively.

To a mixture of intermediate **12a** (or **12b−d**, 1 equiv) and methanesulfonyl chloride (1 equiv) in dichloromethane (5 mL) at 0 °C, triethylamine (1.2 equiv) was dropwise added. The mixture was stirred for 5 h at this temperature and then concentrated under reduced pressure. Water was added, and the residue was filtered, recrystallized from methanol and dried in vacuum to yield target compounds **10d**, **10e** and **11c**, **11d**.

To a mixture of intermediate **12b** (1 equiv) and prepared intermediate **7** (1.2 equiv) in 5 mL of dichloromethane, triethylamine (1.2 equiv) was added. The mixture was stirred at rt for 5 h and then concentrated under reduced pressure to provide the crude intermediate **13**. Without further purification, **13** was directly dissolved in 4 mL of dichloromethane/trifluoroacetic acid (v/v, 1/1) and the reaction

DOI: 10.1021/acs.jmedchem.8b01729
J. Med. Chem. 2019, 62, 2083−2098

mixture was stirred at rt until completion. After removal of the excess solvent under reduced pressure, saturated potassium carbonate aqueous solution was added to the residue. After extraction with EtOAc, the combined organic layers were dried over anhydrous Na_2SO_4, filtered and concentrated under reduced pressure. Then the residue was further purified by silica gel chromatography with methanol/dichloromethane as eluent and recrystallized from methanol to afford the target compound **10f**.

*tert-Butyl(1-(4-((4-(4-cyano-2,6-dimethylphenoxy)pyrimidin-2-yl)amino)benzyl)piperidin-4-yl)carbamate (**10a**).* White solid. Yield: 38%. Decomposed at 118.2 °C. ^{1}H NMR (400 MHz, DMSO-d_6, ppm): δ 9.58 (s, 1H, NH), 8.39 (d, J = 5.52 Hz, 1H, pyrimidine-H), 7.75 (s, 2H, Ph-H), 7.27 (d, J = 5.76 Hz, 2H, Ph-H), 6.94 (d, J = 7.92 Hz, 2H, Ph-H), 6.71 (d, J = 7.40 Hz, 1H, CONH), 6.54 (d, J = 5.48 Hz, 1H, pyrimidine-H), 3.29 (s, 2H, CH_2), 3.20−3.18 (m, 1H, piperidine-H), 2.70−2.68 (m, 2H, piperidine-H), 2.12 (s, 6H, Ph-CH_3 × 2), 1.88 (t, J = 11.04 Hz, 2H, piperidine-H), 1.67−1.65 (m, 2H, piperidine-H), 1.37−1.31 (m, 11H, CH_3 × 3, piperidine-H). ^{13}C NMR (100 MHz, DMSO-d_6, ppm): δ 168.31, 160.96, 160.13, 155.29, 154.01, 139.20, 133.21 (Ph-C × 2), 133.03 (Ph-C × 2), 132.00, 129.14 (Ph-C × 2), 119.06, 118.78 (Ph-C × 2), 108.86, 97.61, 77.86 (quaternary-C), 62.24 (CH_2), 52.48 (piperidine-C × 2), 48.08 (piperidine-C), 32.31 (piperidine-C × 2), 28.74 (CH_3 × 3), 16.28 (Ph-CH_3 × 2). ESI-MS m/z: 529.2919 (M + 1)$^+$, 551.2706 (M + 23)$^+$, $C_{30}H_{36}N_6O_3$, (528.2849).

*tert-Butyl-4-((4-((4-(4-cyano-2,6-dimethylphenoxy)pyrimidin-2-yl)amino)benzyl)amino)piperidine-1-carboxylate (**10b**).* White solid. Yield: 58%. Decomposed at 102.8 °C. ^{1}H NMR (400 MHz, DMSO-d_6, ppm): δ 9.55 (s, 1H, NH), 8.39 (d, J = 5.56 Hz, 1H, pyrimidine-H), 7.74 (s, 2H, Ph-H), 7.25 (d, J = 6.96 Hz, 2H, Ph-H), 7.00 (d, J = 8.32 Hz, 2H, Ph-H), 6.54 (d, J = 5.52 Hz, 1H, pyrimidine-H), 3.81−3.78 (m, 2H, piperidine-H), 3.60 (s, 2H, CH_2), 3.32 (s, 1H, NH), 2.78 (br s, 2H, piperidine-H), 2.14−2.10 (m, 7H, Ph-CH_3 × 2, piperidine-H), 1.78−1.74 (m, 2H, piperidine-H), 1.43−1.39 (m, 11H, CH_3 × 3, piperidine-H). ^{13}C NMR (100 MHz, DMSO-d_6, ppm): δ 168.32, 160.97, 160.12, 154.36, 154.02, 138.90, 133.22 (Ph-C × 2), 133.03 (Ph-C × 2), 130.21, 128.18 (Ph-C × 2), 119.06, 118.73 (Ph-C × 2), 108.86, 97.53, 78.87 (quaternary-C), 56.50, 53.47, 49.72 (piperidine-C × 2), 32.26 (piperidine-C × 2), 28.58 (CH_3 × 3), 16.28 (Ph-CH_3 × 2). ESI-MS m/z: 529.2926 (M + 1)$^+$, 551.2711 (M + 23)$^+$, $C_{30}H_{36}N_6O_3$, (528.2849).

*3,5-Dimethyl-4-((2-((4-(morpholinomethyl)phenyl)amino)-pyrimidin-4-yl)oxy)benzonitrile (**10c**).* White solid. Yield: 65%. mp 147.0−149.1 °C. ^{1}H NMR (400 MHz, DMSO-d_6, ppm): δ 9.60 (s, 1H, NH), 8.40 (d, J = 5.56 Hz, 1H, pyrimidine-H), 7.75 (s, 2H, Ph-H), 7.26 (d, J = 6.96 Hz, 2H, Ph-H), 6.97 (d, J = 8.36 Hz, 2H, Ph-H), 6.56 (d, J = 5.56 Hz, 1H, pyrimidine-H), 3.57 (t, J = 4.56 Hz, 4H, morpholine-H), 3.33 (s, 2H, CH_2), 3.12 (br s, 4H, morpholine-H), 2.11 (s, 6H, Ph-CH_3 × 2). ^{13}C NMR (100 MHz, DMSO-d_6, ppm): δ 168.31, 160.99, 160.10, 154.04, 139.31, 133.23 (Ph-C × 2), 133.01 (Ph-C × 2), 131.09, 129.20 (Ph-C × 2), 119.07, 118.77 (Ph-C × 2), 108.85, 97.62, 66.65 (morpholine-C × 2), 62.46 (CH_2), 53.56 (morpholine-C × 2), 16.27 (Ph-CH_3 × 2). ESI-MS m/z: 416.2080 (M + 1)$^+$, $C_{24}H_{25}N_5O_2$, (415.2008). HPLC purity: 100%.

*3,5-Dimethyl-4-((2-((4-((4-(methylsulfonyl)piperazin-1-yl)-methyl)phenyl)amino)pyrimidin-4-yl)oxy)benzonitrile (**10d**).* White solid. Yield: 62%. Decomposed at 219.6 °C. ^{1}H NMR (400 MHz, DMSO-d_6, ppm): δ 9.61 (s, 1H, NH), 8.40 (d, J = 5.52 Hz, 1H, pyrimidine-H), 7.76 (s, 2H, Ph-H), 7.26 (d, J = 5.36 Hz, 2H, Ph-H), 6.97 (d, J = 8.04 Hz, 2H, Ph-H), 6.56 (d, J = 5.52 Hz, 1H, pyrimidine-H), 3.40 (s, 2H, CH_2), 3.12 (br s, 4H, piperazine-H), 2.87 (s, 3H, SO_2CH_3), 2.41 (br s, 4H, piperazine-H), 2.12 (s, 6H, Ph-CH_3 × 2). ^{13}C NMR (100 MHz, DMSO-d_6, ppm): δ 168.31, 161.01, 160.08, 154.07, 139.38, 133.24 (Ph-C × 2), 133.03 (Ph-C × 2), 131.12, 129.04 (Ph-C × 2), 119.14, 118.79 (Ph-C × 2), 108.83, 97.63, 61.47 (CH_2), 52.14 (piperazine-C × 2), 45.95 (piperazine-C × 2), 34.03 (SO_2CH_3), 16.28 (Ph-CH_3 × 2). ESI-MS m/z: 493.2019 (M + 1)$^+$, 515.1831 (M + 23)$^+$, $C_{25}H_{28}N_6O_3S$, (492.1944).

*N-(1-(4-((4-(4-Cyano-2,6-dimethylphenoxy)pyrimidin-2-yl)-amino)benzyl)piperidin-4-yl)methanesulfonamide (**10e**).* White solid. Yield: 46%. Decomposed at 169.5 °C. ^{1}H NMR (400 MHz, DMSO-d_6, ppm): δ 9.60 (s, 1H, NH), 8.40 (d, J = 5.44 Hz, 1H, pyrimidine-H), 7.75 (s, 2H, Ph-H), 7.30−6.96 (m, 5H, Ph-H, $NHSO_2$), 6.56 (d, J = 4.96 Hz, 1H, pyrimidine-H), 3.32 (s, 2H, CH_2), 3.19−3.01 (m, 1H, piperidine-H), 2.90 (s, 3H, SO_2CH_3), 2.79−2.60 (m, 2H, piperidine-H), 2.12 (s, 6H, Ph-CH_3 × 2), 1.98−1.80 (m, 4H, piperidine-H), 1.59−1.42 (m, 2H, piperidine-H). ^{13}C NMR (100 MHz, DMSO-d_6, ppm): δ 168.32, 160.99, 160.09, 153.99, 133.23 (Ph-C × 2), 133.04 (Ph-C × 2), 129.08 (Ph-C × 2), 119.07, 118.78 (Ph-C × 2), 108.87, 99.99, 97.78, 56.50 (piperidine-C × 2), 52.07, 41.51 (piperidine-C × 2), 33.30 (SO_2CH_3), 16.29 (Ph-CH_3 × 2). ESI-MS m/z: 507.2175 (M + 1)$^+$, 529.1996 (M + 23)$^+$, $C_{26}H_{30}N_6O_3S$, (506.2100).

*N-(1-(4-((4-(4-Cyano-2,6-dimethylphenoxy)pyrimidin-2-yl)-amino)benzyl)piperidin-4-yl)aminosulfonamide (**10f**).* White solid. Two-step yield: 49%. Decomposed at 184.2 °C. ^{1}H NMR (400 MHz, DMSO-d_6, ppm): δ 9.59 (s, 1H, NH), 9.28 (d, J = 7.64 Hz, 1H, $NHSO_2$), 8.40 (d, J = 5.56 Hz, 1H, pyrimidine-H), 7.75 (s, 2H, Ph-H), 7.28 (d, J = 6.60 Hz, 2H, Ph-H), 6.96 (d, J = 8.28 Hz, 2H, Ph-H), 6.55 (d, J = 5.56 Hz, 1H, pyrimidine-H), 3.63−3.56 (m, 1H, piperidine-H), 3.32 (s, 2H, CH_2), 2.77−2.74 (m, 2H, piperidine-H), 2.12 (s, 6H, Ph-CH_3 × 2), 1.93 (t, J = 11.16 Hz, 2H, piperidine-H), 1.72−1.70 (m, 2H, piperidine-H), 1.58−1.50 (m, 2H, piperidine-H). ^{13}C NMR (100 MHz, DMSO-d_6, ppm): δ 168.31, 160.97, 160.12, 154.01, 139.27, 133.22 (Ph-C × 2), 133.03 (Ph-C × 2), 131.76, 129.20 (Ph-C × 2), 119.07, 118.80 (Ph-C × 2), 108.85, 97.65, 62.06 (CH_2), 52.19 (piperidine-C × 2), 48.08 (piperidine-C), 31.10 (piperidine-C × 2), 16.28 (Ph-CH_3 × 2). ESI-MS m/z: 508.2131 (M + 1)$^+$, $C_{25}H_{29}N_7O_3S$, (507.2053).

*tert-Butyl-(E)-4-(4-((4-(4-(2-cyanovinyl)-2,6-dimethylphenoxy)-pyrimidin-2-yl)amino)benzyl)piperazine-1-Carboxylate (**11a**).* White solid. Yield: 46%. mp 161.8−162.3 °C. ^{1}H NMR (400 MHz, DMSO-d_6, ppm): δ 9.57 (s, 1H, NH), 8.37 (d, J = 5.56 Hz, 1H, pyrimidine-H), 7.66 (d, J = 16.64 Hz, 1H, CH═), 7.53 (s, 2H, Ph-H), 7.29 (d, J = 7.12 Hz, 2H, Ph-H), 6.92 (d, J = 8.16 Hz, 2H, Ph-H), 6.50 (d, J = 5.60 Hz, 1H, pyrimidine-H), 6.47 (d, J = 16.68 Hz, 1H, CH═), 3.33−3.30 (m, 6H, CH_2, piperazine-H), 2.24 (t, J = 4.44 Hz, 4H, piperazine-H), 2.09 (s, 6H, Ph-CH_3 × 2), 1.39 (s, 9H, CH_3 × 3). ^{13}C NMR (100 MHz, DMSO-d_6, ppm): δ 168.69, 160.75, 160.15, 154.27, 152.36, 150.52, 139.47, 131.80 (Ph-C × 4), 130.95, 129.21, 128.68 (Ph-C × 2), 119.33, 118.70 (Ph-C × 2), 97.62, 96.74, 79.17 (quaternary-C), 61.99 (CH_2), 56.50 (piperazine-C × 2), 52.72 (piperazine-C × 2), 28.53 (CH_3 × 3), 16.56 (Ph-CH_3 × 2). ESI-MS m/z: 541.2922 (M + 1)$^+$, 563.2715 (M + 23)$^+$, $C_{31}H_{36}N_6O_3$, (540.2849). HPLC purity: 100%.

*tert-Butyl-(E)-(1-(4-((4-(4-(2-cyanovinyl)-2,6-dimethylphenoxy)-pyrimidin-2-yl)amino)benzyl)piperidin-4-yl)carbamate (**11b**).* White solid. Yield: 35%. mp 125.1−126.0 °C. ^{1}H NMR (400 MHz, DMSO-d_6, ppm): δ 9.54 (s, 1H, NH), 8.36 (d, J = 5.56 Hz, 1H, pyrimidine-H), 7.66 (d, J = 16.64 Hz, 1H, CH═), 7.52 (s, 2H, Ph-H), 7.29 (d, J = 6.96 Hz, 2H, Ph-H), 6.91 (d, J = 7.96 Hz, 2H, Ph-H), 6.70 (d, J = 7.16 Hz, 1H, CONH), 6.49 (d, J = 5.80 Hz, 1H, pyrimidine-H), 6.46 (d, J = 16.80 Hz, 1H, CH═), 3.27 (s, 2H, CH_2), 3.20−3.18 (m, 1H, piperidine-H), 2.69−2.66 (m, 2H, piperidine-H), 2.09 (s, 6H, Ph-CH_3 × 2), 1.87 (t, J = 11.12 Hz, 2H, piperidine-H), 1.67−1.64 (m, 2H, piperidine-H), 1.37−1.31 (m, 11H, CH_3 × 3, piperidine-H). ^{13}C NMR (100 MHz, DMSO-d_6, ppm): δ 168.69, 160.73, 160.19, 155.28, 152.33, 150.54, 139.31, 131.80 (Ph-C × 2), 131.77 (Ph-C × 2), 131.39, 129.16, 128.68 (Ph-C × 2), 119.39, 118.75 (Ph-C × 2), 97.62, 96.74, 77.88 (quaternary-C), 62.21 (CH_2), 52.43 (piperidine-C × 2), 48.03 (piperidine-C), 32.32 (piperidine-C × 2), 28.74 (CH_3 × 3), 16.56 (Ph-CH_3 × 2). ESI-MS m/z: 555.3081 (M + 1)$^+$, 577.2881 (M + 23)$^+$, $C_{32}H_{38}N_6O_3$, (554.3005).

*(E)-3-(3,5-Dimethyl-4-((2-((4-((4-(methylsulfonyl)piperazin-1-yl)-methyl)phenyl)amino)pyrimidin-4-yl)oxy)phenyl)acrylonitrile (**11c**).* White solid. Yield: 44%. mp 227.4−228.1 °C. ^{1}H NMR (400 MHz, DMSO-d_6, ppm): δ 9.57 (s, 1H, NH), 8.37 (d, J = 5.60 Hz, 1H, pyrimidine-H), 7.67 (d, J = 16.68 Hz, 1H, CH═), 7.53 (s, 2H, Ph-H), 7.31 (d, J = 7.36 Hz, 2H, Ph-H), 6.93 (d, J = 8.20 Hz, 2H, Ph-H), 6.50 (d, J = 5.80 Hz, 1H, pyrimidine-H), 6.48 (d, J = 16.96 Hz, 1H, CH═), 3.37 (s, 2H, CH_2), 3.10 (t, J = 4.32 Hz, 4H, piperazine-H), 2.88 (s, 3H, SO_2CH_3), 2.39 (br s, 4H, piperazine-H), 2.09 (s, 6H, Ph-CH_3 × 2). ^{13}C NMR (100 MHz, DMSO-d_6, ppm): δ 168.70, 160.76, 160.16, 152.36,

DOI: 10.1021/acs.jmedchem.8b01729
J. Med. Chem. 2019, 62, 2083−2098

150.59, 139.54, 131.81 (Ph-C × 2), 131.79 (Ph-C × 2), 130.89, 129.17 (Ph-C × 2), 128.68 (Ph-C × 2), 119.45, 118.75, 97.65, 96.71, 61.60 (CH_2), 52.15 (piperazine-C × 2), 45.94 (piperazine-C × 2), 34.16 (SO_2CH_3), 16.56 (Ph-CH_3 × 2). ESI-MS *m/z*: 519.2176 $(M + 1)^+$, 541.1993 $(M + 23)^+$, $C_{27}H_{30}N_6O_3S$, (518.2100). HPLC purity: 100%.

*(E)-N-(1-(4-((4-(4-(2-Cyanovinyl)-2,6-dimethylphenoxy)-pyrimidin-2-yl)amino)benzyl)piperidin-4-yl)methanesulfonamide (**11d**).* White solid, Yield: 51%. Decomposed at 218.0 °C. ^{1}H NMR (400 MHz, DMSO-d_6, ppm): δ 9.54 (s, 1H, NH), 8.37 (d, *J* = 5.56 Hz, 1H, pyrimidine-H), 7.66 (d, *J* = 16.68 Hz, 1H, CH═), 7.52 (s, 2H, Ph-H), 7.30 (d, *J* = 7.08 Hz, 2H, Ph-H), 7.01 (d, *J* = 7.24 Hz, 1H, $NHSO_2$), 6.91 (d, *J* = 8.12 Hz, 2H, Ph-H), 6.49 (d, *J* = 5.72 Hz, 1H, pyrimidine-H), 6.46 (d, *J* = 16.80 Hz, 1H, CH═), 3.28 (s, 2H, CH_2), 3.12−3.04 (m, 1H, piperidine-H), 2.90 (s, 3H, SO_2CH_3), 2.69−2.66 (m, 2H, piperidine-H), 2.09 (s, 6H, Ph-CH_3 × 2), 1.95−1.90 (m, 2H, piperidine-H), 1.80−1.77 (m, 2H, piperidine-H), 1.47−1.38 (m, 2H, piperidine-H). ^{13}C NMR (100 MHz, DMSO-d_6, ppm): δ 168.69, 160.74, 160.19, 152.34, 150.54, 139.32, 131.80 (Ph-C × 2), 131.77 (Ph-C × 2), 131.67, 129.15, 128.68 (Ph-C × 2), 119.39, 118.77 (Ph-C × 2), 97.62, 96.73, 62.09 (CH_2), 52.11 (piperidine-C × 2), 50.79 (piperidine-C), 41.56 (piperidine-C × 2), 33.37 (SO_2CH_3), 16.56 (Ph-CH_3 × 2). ESI-MS *m/z*: 533.2334 $(M + 1)^+$, 555.2153 $(M + 23)^+$, $C_{28}H_{32}N_6O_3S$, (532.2257). HPLC purity: 98.30%.

*3,5-Dimethyl-4-((2-((4-(piperazin-1-ylmethyl)phenyl)amino)-pyrimidin-4-yl)oxy)benzonitrile (**12a**).* White solid. Yield: 65%. ESI-MS *m/z*: 415.5 $(M + 1)^+$, $C_{24}H_{26}N_6O$, (414.22).

*4-((2-((4-((4-Aminopiperidin-1-yl)methyl)phenyl)amino)-pyrimidin-4-yl)oxy)-3,5-dimethylbenzonitrile (**12b**).* White solid. Yield: 54%. ESI-MS *m/z*: 429.5 $(M + 1)^+$, $C_{25}H_{28}N_6O$, (428.23).

*(E)-3-(3,5-Dimethyl-4-((2-((4-(piperazin-1-ylmethyl)phenyl)-amino)pyrimidin-4-yl)oxy)phenyl)acrylonitrile (**12c**).* White solid. Yield: 42%. mp 139.5−141.1 °C. ESI-MS *m/z*: 441.2398 $(M + 1)^+$, $C_{26}H_{28}N_6O$, (440.2325).

*(E)-3-(4-((2-((4-((4-Aminopiperidin-1-yl)methyl)phenyl)amino)-pyrimidin-4-yl)oxy)-3,5-dimethylphenyl)acrylonitrile (**12d**).* White solid. Yield: 58%. mp 138.2−139.8 °C. ESI-MS *m/z*: 455.2548 $(M + 1)^+$, $C_{27}H_{30}N_6O$, (454.2481).

Preparation of Target Compound 17. To a solution of 2,4,6-trimethylphenol (0.14 g, 1 mmol) and potassium carbonate (0.17 g, 1.2 mmol) in 4 mL of DMF, 2,4,6-trichloro-1,3,5-triazine **14** (0.18 g, 1 mmol) was added, and the mixture was stirred at 50 °C until completion. Water was added, and the mixture was extracted with EtOAc. The combined organic layers were washed with saturated brine, dried over anhydrous Na_2SO_4, filtered, and concentrated under reduced pressure to provide the crude intermediate **15**. **15** was used in next step without further purification.

Intermediate **15** (0.28 g, 1 mmol), intermediate **5c** (0.19 g, 1 mmol), and sodium bicarbonate (0.084 g, 1 mmol) were dissolved in 6 mL of mixed solvent [tetrahydrofuran (THF)/acetone/water = 4/1/1] and the reaction mixture was stirred at rt for 2 h. The excess solvent was removed under reduced pressure, and water was added to the residue. The mixture was extracted with EtOAc, and the combined organic layers were dried over anhydrous Na_2SO_4, filtered, concentrated under reduced pressure, and finally recrystallized from methanol to afford the key intermediate **16**. White solid. Decomposed at 184.2 °C. ESI-MS *m/z*: 440.1855 $(M + 1)^+$, $C_{23}H_{26}ClN_5O_2$, (439.1775).

Intermediate **16** (0.09 g, 0.20 mmol) was dissolved in ammonia water/1,4-dioxane (4 mL, v/v, 1/1) in a sealed tube, and then the mixture was heated at 100 °C for 3 h. The reaction solution was left to cool to rt and filtered. The resulted solid was washed with water and recrystallized using methanol to provide the target compound **17**.

*6-(Mesityloxy)-N^2-(4-(morpholinomethyl)phenyl)-1,3,5-triazine-2,4-diamine (**17**).* White solid. Yield: 66%. Decomposed at 226.9 °C. ^{1}H NMR (400 MHz, DMSO-d_6, ppm): δ 9.42 (s, 1H, NH), 7.56 (br s, 2H, NH_2), 7.15−6.99 (m, 4H, Ph-H), 6.90 (s, 2H, Ph-H), 3.55 (t, 4H, *J* = 4.04 Hz, morpholine-H), 3.36 (s, 2H, CH_2), 2.31 (br s, 4H, morpholine-H), 2.25 (s, 3H, CH_3), 2.04 (s, 6H, CH_3 × 2). ^{13}C NMR (100 MHz, DMSO-d_6, ppm): δ 170.49, 168.90, 166.03, 147.69, 139.06, 134.35, 131.65, 130.13 (Ph-C × 2), 129.38 (Ph-C × 2), 129.35 (Ph-C × 2), 120.13 (Ph-C × 2), 66.69 (morpholine-C × 2), 62.48 (CH_2), 53.57 (morpholine-C × 2), 20.79 (CH_3), 16.54 (CH_3 × 2). ESI-MS *m/z*: 421.2349 $(M + 1)^+$, $C_{23}H_{28}N_6O_2$, (420.2274).

In Vitro Anti-HIV Assays. Evaluation of the antiviral activity and cytotoxicity of the synthesized compounds was performed using the MTT assay as previously described.[22] Stock solutions (10 × final concentration) of test compounds were added in 25 μL volumes to two series of triplicate wells to allow simultaneous evaluation of their effects on mock- and HIV-infected cells at the beginning of each experiment. Serial five-fold dilutions of test compounds were made directly in flat-bottomed 96-well microtiter trays by adding 100 μL medium to the 25 μL stock solution and transferring 25 μL of this solution to another well that contained 100 μL medium using a Biomek 3000 robot (Beckman Instruments, Fullerton, CA). Untreated control HIV- and mock-infected cell samples were included for each sample. HIV-1 WT strain (III_B), HIV-1 drug-resistant strains including K103N/Y181C double mutant strain (RES056), E138K, L100I, K103N, Y181C, Y188L, and F227L + V106A or HIV-2 strain (ROD) stock (50 μL) at 100−300 CCID50 (50% cell culture infectious dose) or culture medium was added to either the infected or mock-infected wells of the microtiter tray. Mock-infected cells were used to evaluate the effect of test compounds on uninfected cells in order to assess its cytotoxicity. Exponentially growing MT-4 cells were centrifuged for 5 min at 1000 rpm and the supernatant was discarded. The MT-4 cells were resuspended at 6×10^5 cells/mL, and 50 μL volumes were transferred to the microtiter tray wells. Five days after infection, the viability of mock- and HIV-infected cells was examined spectrophotometrically by the MTT method. The 50% cytotoxic concentration (CC_{50}) was defined as the concentration of the test compound that reduced the viability of the mock-infected MT-4 cells by 50%. The concentration achieving 50% protection from the cytopathic effect of the virus in infected cells was defined as the 50% effective concentration (EC_{50}).

HIV-1 RT Inhibition Assays. Recombinant WT p66/p51 HIV-1 RT was expressed and purified as described by the report.[30] The RT assay is performed with the EnzChek Reverse Transcriptase Assay kit (Molecular Probes, Invitrogen), as described by the manufacturer. The assay is based on the dsDNA quantitation reagent PicoGreen. This reagent shows a pronounced increase in fluorescence signal upon binding to dsDNA or RNA-DNA heteroduplexes. Single-stranded nucleic acids generate only minor fluorescence signal enhancement when a sufficiently high dye: base pair ratio is applied.[31] This condition is met in the assay.

A poly(rA) template of approximately 350 bases long and an oligo(dT)16 primer are annealed in a molar ratio of 1:1.2 (60 min at rt). RNA/DNA (52 ng) is brought into each well of a 96-well plate in a volume of 20 μL polymerization buffer [60 mM Tris-HCl, 60 mM KCl, 8 mM $MgCl_2$, 13 mM dithiothreitol (DTT), 100 μM dTTP, pH 8.1]. RT enzyme solution, 5 μL, diluted to a suitable concentration in enzyme dilution buffer (50 mM Tris-HCl, 20% glycerol, 2 mM DTT, pH 7.6), is added. The reactions are incubated at 25 °C for 40 min and then stopped by the addition of ethylenediaminetetraacetate (15 mM fc). Heteroduplexes are then detected by addition of PicoGreen. Signals are read using an excitation wavelength of 490 nm and emission detection at 523 nm using a spectrofluorometer (Safire2, Tecan). To test the activity of compounds against RT, 1 μL of compound in DMSO is added to each well before the addition of RT enzyme solution. Control wells without compound contain the same amount of DMSO. Results are expressed as relative fluorescence, that is, the fluorescence signal of the reaction mix with compound divided by the signal of the same reaction mix without compound.

Docking and MD Simulation Studies. Molecular docking study was performed to investigate the binding mode of selected ligands with the WT HIV-1 RT enzyme and its E138K and K103N variants using Glide. The three-dimensional structure of the HIV-1 RT enzyme (PDB code 3M8Q)[23] was downloaded from the Protein Data Bank (https://www.rcsb.org).[32] The PDB entries 3MED[33] and 2HNY,[34] representative for the HIV-1 RT E138K and K103N mutants bound to ETR and NVP, respectively, were used as a template to generate the proper spatial arrangement of Asn103 ($3M8Q_{K103N}$) and Lys138 ($3M8Q_{E138K}$) in the WT 3M8Q structure. This strategy was motivated by the low rmsd determined for heavy atoms with regard to structure 3M8Q (rmsd

DOI: 10.1021/acs.jmedchem.8b01729
J. Med. Chem. 2019, 62, 2083−2098

of 0.7 and 1.7 Å for 3MED and 2HNY, respectively, and 0.6 (3MED) (2HNY) and 1.4 Å for the subset of residues located at 10 Å of the ligand DJZ in 3M8Q, chosen as those shaping the binding pocket; Supporting Information Table S1). Furthermore, there are slight, but critical conformational differences in the loops that shape the tolerant region I in 3MED, 3MEC, and 2HNY, which would pose additional challenges for the success of docking calculations in predicting the ligand pose, thus making the usage of 3M8Q better suited as a template to build the $3M8Q_{K103N}$ and $3M8Q_{E138K}$ mutated variants. Finally, the potential effect on the docked poses of ligands due to the structural water molecule 567 was also examined. Overall, a total of 6 protein structures were considered in docking calculations (WT and K103N and E138K variants, with and without water molecule 567).

Proteins and ligands were prepared with Maestro.[35] A flexible docking run with a core constraint was performed. To this end, the 4-(2,6-dimethylphenoxy)pyrimidin-2-amine moiety of the crystallographic ligand in 3M8Q was used as a core constraint. Pose search as well as binding affinities were evaluated by applying the standard precision function implemented in Glide. A distance-dependent dielectric constant of 2.0 was used, and the standard vdW scaling factor of the ligand nonpolar atoms with a partial charge lower than 0.15 was reduced to 0.90. A maximum number of minimization steps of 100 was applied after docking to refine the previously found poses. A maximum of 5 poses was generated for each ligand.

The stability of the docked poses was examined by means of unbiased MD simulations using Amber16.[36] The protein was described using the ff99SB-ILDN force field,[37,38] and the protonation state of ionizable residues was checked by means of PROPKA calculations.[39] The ligand was parametrized using the general Amber (GAFF) force field[40] and restrained electrostatic potential partial charges[41] were derived at the B3LYP/6-31G(d) level, after preliminary geometry optimization of the compound with Gaussian 09.[42] Each protein−ligand complex was solvated with a truncated octahedral box of TIP3P[43] water molecules (layer of 18 Å) and neutralized by adding chloride counterions, leading to a simulated system that consists around 42200 atoms.

For each simulated system, energy minimization was applied to hydrogen atoms, then to water molecules, and finally to the whole system using a combination of 2000 cycles of steepest descent method and 8000 steps of conjugate gradient. Heating to 300 K was completed in five steps (50 ps/step), the first being performed at constant volume and the rest at constant pressure, followed by a last step (5 ns) also a constant pressure. Harmonic restraints with a force constant of 10 kcal mol^{-1} $Å^{-2}$ were applied to selected interactions of the ligand to avoid artifactual changes in the binding mode. These restraints were gradually reduced along the first 30 ns of MD simulation, and the system was allowed to evolve without restraints for 100 ns of MD production at 300 K. MD simulations were performed using SHAKE[44] to constrain bonds involving hydrogen atoms, in conjunction with periodic boundary conditions at constant volume, a cut-off of 10 Å for nonbonded interactions, and the particle mesh Ewald method beyond the cut-off distance.[45] The analysis of the trajectories was performed for snapshots collected every 2 ps.

Water Solubility Measurement. Compound **10c** or **11c** (1 mg) was dissolved in deionized water until the solution was clear. The assays were measured at least in duplicate.

CYP Enzymatic Inhibitory Activity Assay. The CYP enzymatic inhibitory activity was determined by WuXi AppTec (Shanghai) Co., Ltd, China. Compound **11c** was prepared at eight concentrations (0, 0.05, 0.15, 0.5, 1.5, 5.0, 15, and 50 μM) and then was incubated with human liver microsomes (0.1 mg/mL) and cofactor reduced nicotinamide adenine dinucleotide phosphate (1 mM) in the presence of the corresponding probe substrates (CYP2C9_diclofenac, CYP2C19_S-mephenytoin, CYP2D6_dextromethorphan, CYP3A4_midazolam, and CYP3A4_testosterone, respectively) for 3−20 min (3 min for 3A4 (midazolam), 10 min for CYP2C9 and 3A4 (testosterone), and 20 min for CYP2C19 and CYP2D6) at 37 ± 0.2 °C. The selective CYP inhibitors, sulfaphenazole (CYP2C9), (+)-*N*-3-benzylnirvanol (CYP2C19), quinidine (CYP2D6), and ketoconazole (CYP3A4), were screened as positive controls. Cold acetonitrile solution (400 μL) containing 200 ng/mL tolbutamide and 200 ng/mL labetalol was used for terminating the reaction. The sample solutions were centrifuged at 4000 rpm for 20 minutes to precipitate protein, and then 200 μL of the supernatant was diluted with 100 μL HPLC water and was shaken for 10 min. Finally, the mixtures were sent to LC-MS/MS analysis.

Acute Toxicity Assessment. All animal treatments were performed strictly in accordance with the institutional guidelines of Animal Care and Use Committee at Shandong University, after gaining approval from the Animal Ethical and Welfare Committee (AEWC). We performed this study with an authorized standard method to detect acute toxicity using mice and accredited by Laboratory Animal Ethical and Welfare Committee of Shandong University Cheeloo College of Medicine. Compound **11c** was first suspended in 80% PEG400 solution. Six male and six female Kunming mice (18−22 g) were purchased from the animal experimental center of Shandong University and were randomly divided into four groups (n = 3): male control group, female control group, male test group, and female test group. All mice had been fasted for 12 h, and then the mice in test groups were administered intragastrically by gavage at a dose of 2000 $mg{\cdot}kg^{-1}$ of **11c** while the mice in control groups were administered with the same volume of vehicle solution on the first day. The death, abnormal behaviors, and body weight of these mice were monitored every day during the subsequent 1 week.

Subacute Toxicity Assessment. Another batch of eight male and eight female Kunming mice (also purchased from the animal experimental center of Shandong University) were randomly divided into four groups (n = 4): male control group, female control group, male test group, and female test group. All mice had been fasted for 12 h, and then the mice in test groups were po administrated with a dose of 50 $mg{\cdot}kg^{-1}$ of **11c** once every other day for 14 days (D0, D2, D4, D6, D8, D10, and D12), while the mice in control groups were administered with the same volume of vehicle solution. The body weight of the mice was measured before administrating each time. All of the mice were dissected at D14, and the heart, liver, spleen, lung, and kidney were extracted. These organs were then examined by HE to see if any damage occurred.

■ ASSOCIATED CONTENT

Supporting Information

The Supporting Information is available free of charge on the ACS Publications website at DOI: 10.1021/acs.jmedchem.8b01729.

ESI-MS, ^{1}H NMR, and ^{13}C NMR spectra for representative target compounds and selected representations of the binding mode of ligands from docking and MD simulations (PDF)

Molecular formula strings (CSV)

■ AUTHOR INFORMATION

Corresponding Authors

*E-mail: christophe.pannecouque@rega.kuleuven.be. Phone: 32-(0)16-332171 (C.P.).

*E-mail: zhanpeng1982@sdu.edu.cn. Phone: 086-531-88382005 (P.Z.).

*E-mail: xinyongl@sdu.edu.cn. Phone: 086-531-88380270 (X.L.).

ORCID

Boshi Huang: 0000-0003-2243-1947

Francisco Javier Luque: 0000-0002-8049-3567

Dongwei Kang: 0000-0001-9232-953X

Jian Zhang: 0000-0002-5668-2974

Peng Zhan: 0000-0002-9675-6026

Present Addresses

⊥Department of Medicinal Chemistry, School of Pharmacy, Virginia Commonwealth University, 800 E Leigh Street, Richmond, VA 23298, United States.

DOI: 10.1021/acs.jmedchem.8b01729
J. Med. Chem. 2019, 62, 2083−2098

[#]Department of Medicinal Chemistry, College of Pharmacy, University of Michigan, 1600 Huron Parkway, Ann Arbor, MI 48109, USA.

Notes

The authors declare no competing financial interest.

■ ACKNOWLEDGMENTS

The financial support from the National Natural Science Foundation of China (NSFC no. 81273354), Key Project of NSFC for International Cooperation (no. 81420108027), Young Scholars Program of Shandong University (YSPSDU, no. 2016WLJH32), Key research and development project of Shandong Province (no. 2017CXGC1401), Major Project of Science and Technology of Shandong Province (no. 2015ZDJS04001), Spanish Ministerio de Economía y Competitividad (SAF2017-88107-R, MDM-2017-0767), Generalitat de Catalunya (2017SGR1746), and KU Leuven (GOA 10/014) is gratefully acknowledged. We thank K. Erven, K. Uyttersprot and C. Heens for technical assistance with the HIV assays. We are also very grateful to Doctor Jiaxiang Lin at Department of Pathology, Jinan Maternity And Child Care Hospital, for her critical examination on the extracted organs of dissected mice.

■ ABBREVIATIONS

HIV, human immunodeficiency virus; RT, reverse transcriptase; NNRTIs, non-nucleoside reverse transcriptase inhibitors; NNIBP, NNRTI binding pocket; HAART, highly active antiretroviral therapy; RAMs, resistance-associated mutations; DAPY, diarylpyrimidine; WT, wild-type; SARs, structure−activity relationships; Boc, *t*-butyloxy carbonyl; HRMS, high-resolution mass spectrum; ^{1}H NMR, proton nuclear magnetic resonance; ^{13}C NMR, carbon nuclear magnetic resonance; HPLC, high performance liquid chromatography; MTT, 3-(4,5-dimethyl-2-thiazolyl)-2,5-diphenyl-2-H-tetrazolium bromide; 3TC, lamividine; AZT, zidovudine; NVP, nevirapine; EFV, efavirenz; ETR, etravirine; RPV, rilpivirine; EC_{50}, 50% effective concentration; CC_{50}, 50% cytotoxicity concentration; SI, selectivity index; IC_{50}, 50% inhibition concentration; CV, cyanovinyl; PDB, protein data bank; MD, molecular dynamics; rmsd, root-mean-square deviation; PSA, polar surface area; LE, ligand efficiency; LLE, ligand-lipophilicity efficiency; CYP, cytochrome P450; DDI, drug−drug interactions; HE, hematoxylin−eosin

■ REFERENCES

(1) Zhan, P.; Chen, X.; Li, D.; Fang, Z.; De Clercq, E.; Liu, X. HIV-1 NNRTIs: structural diversity, pharmacophore similarity, and implications for drug design. *Med. Res. Rev.* **2013**, *33*, E1−E72.

(2) Kang, D.; Fang, Z.; Huang, B.; Lu, X.; Zhang, H.; Xu, H.; Huo, Z.; Zhou, Z.; Yu, Z.; Meng, Q.; Wu, G.; Ding, X.; Tian, Y.; Daelemans, D.; De Clercq, E.; Pannecouque, C.; Zhan, P.; Liu, X. Structure-based optimization of thiophene[3,2-d]pyrimidine derivatives as potent HIV-1 non-nucleoside reverse transcriptase inhibitors with improved potency against resistance-associated variants. *J. Med. Chem.* **2017**, *60*, 4424−4443.

(3) Kang, D.; Fang, Z.; Li, Z.; Huang, B.; Zhang, H.; Lu, X.; Xu, H.; Zhou, Z.; Ding, X.; Daelemans, D.; De Clercq, E.; Pannecouque, C.; Zhan, P.; Liu, X. Design, synthesis, and evaluation of thiophene[3,2-d]pyrimidine derivatives as HIV-1 non-nucleoside reverse transcriptase inhibitors with significantly improved drug resistance profiles. *J. Med. Chem.* **2016**, *59*, 7991−8007.

(4) Huang, B.; Li, C.; Chen, W.; Liu, T.; Yu, M.; Fu, L.; Sun, Y.; Liu, H.; De Clercq, E.; Pannecouque, C.; Balzarini, J.; Zhan, P.; Liu, X. Fused heterocycles bearing bridgehead nitrogen as potent HIV-1 NNRTIs. Part 3: optimization of [1,2,4]triazolo[1,5-a]pyrimidine core via structure-based and physicochemical property-driven approaches. *Eur. J. Med. Chem.* **2015**, *92*, 754−765.

(5) Huang, B.; Liang, X.; Li, C.; Chen, W.; Liu, T.; Li, X.; Sun, Y.; Fu, L.; Liu, H.; De Clercq, E.; Pannecouque, C.; Zhan, P.; Liu, X. Fused heterocycles bearing bridgehead nitrogen as potent HIV-1 NNRTIs. Part 4: design, synthesis and biological evaluation of novel imidazo[1,2-a]pyrazines. *Eur. J. Med. Chem.* **2015**, *93*, 330−337.

(6) Huang, B.; Kang, D.; Yang, J.; Zhan, P.; Liu, X. Novel diarylpyrimidines and diaryltriazines as potent HIV-1 NNRTIs with dramatically improved solubility: a patent evaluation of US20140378443A1. *Expert Opin. Ther. Pat.* **2016**, *26*, 281−289.

(7) Bollini, M.; Cisneros, J. A.; Spasov, K. A.; Anderson, K. S.; Jorgensen, W. L. Optimization of diarylazines as anti-HIV agents with dramatically enhanced solubility. *Bioorg. Med. Chem. Lett.* **2013**, *23*, 5213−5216.

(8) Steegen, K.; Bronze, M.; Papathanasopoulos, M. A.; van Zyl, G.; Goedhals, D.; Variava, E.; MacLeod, W.; Sanne, I.; Stevens, W. S.; Carmona, S. HIV-1 antiretroviral drug resistance patterns in patients failing NNRTI-based treatment: results from a national survey in South Africa. *J. Antimicrob. Chemother.* **2017**, *72*, 210−219.

(9) Asahchop, E. L.; Oliveira, M.; Wainberg, M. A.; Brenner, B. G.; Moisi, D.; Toni, T. d. A.; Tremblay, C. L. Characterization of the E138K resistance mutation in HIV-1 reverse transcriptase conferring susceptibility to etravirine in B and non-B HIV-1 subtypes. *Antimicrob. Agents Chemother.* **2011**, *55*, 600−607.

(10) Xu, H.-T.; Colby-Germinario, S. P.; Asahchop, E. L.; Oliveira, M.; McCallum, M.; Schader, S. M.; Han, Y.; Quan, Y.; Sarafianos, S. G.; Wainberg, M. A. Effect of mutations at position E138 in HIV-1 reverse transcriptase and their interactions with the M184I mutation on defining patterns of resistance to nonnucleoside reverse transcriptase inhibitors rilpivirine and etravirine. *Antimicrob. Agents Chemother.* **2013**, *57*, 3100−3109.

(11) Bradshaw, D.; Mandalia, S.; Nelson, M. How common is the non-nucleoside reverse transcriptase inhibitor mutation E138K in clinical practice? *J. Infect.* **2011**, *63*, 172−173.

(12) Wainberg, M. Combination therapies, effectiveness, and adherence in patients with HIV infection: clinical utility of a single tablet of emtricitabine, rilpivirine, and tenofovir. *HIV AIDS Res. Palliat. Care* **2013**, *5*, 41−49.

(13) Chen, W.; Zhan, P.; Daelemans, D.; Yang, J.; Huang, B.; De Clercq, E.; Pannecouque, C.; Liu, X. Structural optimization of pyridine-type DAPY derivatives to exploit the tolerant regions of the NNRTI binding pocket. *Eur. J. Med. Chem.* **2016**, *121*, 352−363.

(14) Chen, X.; Zhan, P.; Liu, X.; Cheng, Z.; Meng, C.; Shao, S.; Pannecouque, C.; Clercq, E. D.; Liu, X. Design, synthesis, anti-HIV evaluation and molecular modeling of piperidine-linked amino-triazine derivatives as potent non-nucleoside reverse transcriptase inhibitors. *Bioorg. Med. Chem.* **2012**, *20*, 3856−3864.

(15) Zhang, L.; Zhan, P.; Chen, X.; Li, Z.; Xie, Z.; Zhao, T.; Liu, H.; De Clercq, E.; Pannecouque, C.; Balzarini, J.; Liu, X. Design, synthesis and preliminary SAR studies of novel N-arylmethyl substituted piperidine-linked aniline derivatives as potent HIV-1 NNRTIs. *Bioorg. Med. Chem.* **2014**, *22*, 633−642.

(16) Engelhart, C. A.; Aldrich, C. C. Synthesis of chromone, quinolone, and benzoxazinone sulfonamide nucleosides as conformationally constrained inhibitors of adenylating enzymes required for siderophore biosynthesis. *J. Org. Chem.* **2013**, *78*, 7470−7481.

(17) Tian, Y.; Du, D.; Rai, D.; Wang, L.; Liu, H.; Zhan, P.; De Clercq, E.; Pannecouque, C.; Liu, X. Fused heterocyclic compounds bearing bridgehead nitrogen as potent HIV-1 NNRTIs. Part 1: design, synthesis and biological evaluation of novel 5,7-disubstituted pyrazolo[1,5-a]pyrimidine derivatives. *Bioorg. Med. Chem.* **2014**, *22*, 2052−2059.

(18) Chen, X.; Liu, X.; Meng, Q.; Wang, D.; Liu, H.; De Clercq, E.; Pannecouque, C.; Balzarini, J.; Liu, X. Novel piperidinylamino-diarylpyrimidine derivatives with dual structural conformations as potent HIV-1 non-nucleoside reverse transcriptase inhibitors. *Bioorg. Med. Chem. Lett.* **2013**, *23*, 6593−6597.

DOI: 10.1021/acs.jmedchem.8b01729
J. Med. Chem. 2019, 62, 2083−2098

(19) Park, W. K. C.; Kennedy, R. M.; Larsen, S. D.; Miller, S.; Roth, B. D.; Song, Y.; Steinbaugh, B. A.; Sun, K.; Tait, B. D.; Kowala, M. C.; Trivedi, B. K.; Auerbach, B.; Askew, V.; Dillon, L.; Hanselman, J. C.; Lin, Z.; Lu, G. H.; Robertson, A.; Sekerke, C. Hepatoselectivity of statins: design and synthesis of 4-sulfamoyl pyrroles as HMG-CoA reductase inhibitors. *Bioorg. Med. Chem. Lett.* **2008**, *18*, 1151−1156.
(20) Johnson, T. W.; Richardson, P. F.; Bailey, S.; Broun, A.; Burke, B. J.; Collins, M. R.; Cui, J. J.; Deal, J. G.; Deng, Y.-L.; Dinh, D.; Engstrom, L. D.; He, M.; Hoffman, J.; Hoffman, R. L.; Huang, Q.; Kania, R. S.; Kath, J. C.; Lam, H.; Lam, J. L.; Le, P. T.; Lingardo, L.; Liu, W.; McTigue, M.; Palmer, C. L.; Sach, N. W.; Smeal, T.; Smith, G. L.; Stewart, A. E.; Timofeevski, S.; Zhu, H.; Zhu, J.; Zou, H. Y.; Edwards, M. P. Discovery of (10R)-7-amino-12-fluoro-2,10,16-trimethyl-15-oxo-10,15,16,17-tetrahydro-2H-8,4-(metheno)pyrazolo[4,3-h][2,5,11]-benzoxadiazacyclotetradecine-3-carbonitrile (PF-06463922), a macrocyclic inhibitor of anaplastic lymphoma kinase (ALK) and c-ros oncogene 1 (ROS1) with preclinical brain exposure and broad-spectrum potency against ALK-resistant mutations. *J. Med. Chem.* **2014**, *57*, 4720−4744.
(21) Huang, B.; Wang, X.; Liu, X.; Chen, Z.; Li, W.; Sun, S.; Liu, H.; Daelemans, D.; De Clercq, E.; Pannecouque, C.; Zhan, P.; Liu, X. Discovery of novel DAPY-IAS hybrid derivatives as potential HIV-1 inhibitors using molecular hybridization based on crystallographic overlays. *Bioorg. Med. Chem.* **2017**, *25*, 4397−4406.
(22) Pannecouque, C.; Daelemans, D.; De Clercq, E. Tetrazolium-based colorimetric assay for the detection of HIV replication inhibitors: revisited 20 years later. *Nat. Protoc.* **2008**, *3*, 427−434.
(23) Kertesz, D. J.; Brotherton-Pleiss, C.; Yang, M.; Wang, Z.; Lin, X.; Qiu, Z.; Hirschfeld, D. R.; Gleason, S.; Mirzadegan, T.; Dunten, P. W.; Harris, S. F.; Villaseñor, A. G.; Hang, J. Q.; Heilek, G. M.; Klumpp, K. Discovery of piperidin-4-yl-aminopyrimidines as HIV-1 reverse transcriptase inhibitors. *N*-benzyl derivatives with broad potency against resistant mutant viruses. *Bioorg. Med. Chem. Lett.* **2010**, *20*, 4215−4218.
(24) (a) Yang, H.; Wang, H.-W.; Zhu, T.-W.; Yu, L.-M.; Chen, J.-W.; Wang, L.-X.; Shi, L.; Li, D.; Gu, L.-Q.; Huang, Z.-S.; An, L.-K. Syntheses and antibacterial activity of soluble 9-bromo substituted indolizinoquinoline-5,12-dione derivatives. *Eur. J. Med. Chem.* **2017**, *127*, 166−173. (b) Ndungu, J. M.; Krumm, S. A.; Yan, D.; Arrendale, R. F.; Reddy, G. P.; Evers, T.; Howard, R.; Natchus, M. G.; Saindane, M. T.; Liotta, D. C.; Plemper, R. K.; Snyder, J. P.; Sun, A. Non-nucleoside inhibitors of the measles virus RNA-dependent RNA polymerase: synthesis, structure-activity relationships, and pharmacokinetics. *J. Med. Chem.* **2012**, *55*, 4220−4230. (c) Bollini, M.; Frey, K. M.; Cisneros, J. A.; Spasov, K. A.; Das, K.; Bauman, J. D.; Arnold, E.; Anderson, K. S.; Jorgensen, W. L. Extension into the entrance channel of HIV-1 reverse transcriptase-crystallography and enhanced solubility. *Bioorg. Med. Chem. Lett.* **2013**, *23*, 5209−5212. (d) Bamborough, P.; Diallo, H.; Goodacre, J. D.; Gordon, L.; Lewis, A.; Seal, J. T.; Wilson, D. M.; Woodrow, M. D.; Chung, C.-w. Fragment-based discovery of bromodomain inhibitors part 2: optimization of phenylisoxazole sulfonamides. *J. Med. Chem.* **2012**, *55*, 587−596.
(25) Ertl, P.; Rohde, B.; Selzer, P. Fast calculation of molecular polar surface area as a sum of fragment-based contributions and its application to the prediction of drug transport properties. *J. Med. Chem.* **2000**, *43*, 3714−3717.
(26) Ertl, P. Polar Surface Area In Molecular Drug Properties. In *Methods and Principles in Medicinal Chemistry*; Mannhold, R., Kubinyi, H., Folkers, G., Eds.; Wiley-VCH: Weinheim, 2008; Chapter 5, pp 111−126.
(27) Weuts, I.; Van Dycke, F.; Voorspoels, J.; De Cort, S.; Stokbroekx, S.; Leemans, R.; Brewster, M. E.; Xu, D.; Segmuller, B.; Turner, Y. T. A.; Roberts, C. J.; Davies, M. C.; Qi, S.; Craig, D. Q. M.; Reading, M. Physicochemical properties of the amorphous drug, cast films, and spray dried powders to predict formulation probability of success for solid dispersions: etravirine. *J. Pharm. Sci.* **2011**, *100*, 260−274.
(28) Bertz, R. J.; Granneman, G. R. Use of in vitro and in vivo data to estimate the likelihood of metabolic pharmacokinetic interactions. *Clin. Pharmacokinet.* **1997**, *32*, 210−258.
(29) Cohen, L. H.; Remley, M. J.; Raunig, D.; Vaz, A. D. N. In vitro drug interactions of cytochrome P450: an evaluation of fluorogenic to conventional substrates. *Drug Metab. Dispos.* **2003**, *31*, 1005−1015.
(30) Rawal, R. K.; Tripathi, R.; Katti, S. B.; Pannecouque, C.; De Clercq, E. Design, synthesis, and evaluation of 2-aryl-3-heteroaryl-1,3-thiazolidin-4-ones as anti-HIV agents. *Bioorg. Med. Chem.* **2007**, *15*, 1725−1731.
(31) Rawal, R. K.; Tripathi, R.; Katti, S. B.; Pannecouque, C.; De Clercq, E. Design and synthesis of 2-(2,6-dibromophenyl)-3-heteroaryl-1,3-thiazolidin-4-ones as anti-HIV agents. *Eur. J. Med. Chem.* **2008**, *43*, 2800−2806.
(32) Berman, H. M.; Westbrook, J.; Feng, Z.; Gilliland, G.; Bhat, T. N.; Weissig, H.; Shindyalov, I. N.; Bourne, P. E. The Protein Data Bank. *Nucleic Acids Res.* **2000**, *28*, 235−242.
(33) Lansdon, E. B.; Brendza, K. M.; Hung, M.; Wang, R.; Mukund, S.; Jin, D.; Birkus, G.; Kutty, N.; Liu, X. Crystal structures of HIV-1 reverse transcriptase with etravirine (TMC125) and rilpivirine (TMC278): implications for drug design. *J. Med. Chem.* **2010**, *53*, 4295−4299.
(34) Ren, J.; Nichols, C. E.; Stamp, A.; Chamberlain, P. P.; Ferris, R.; Weaver, K. L.; Short, S. A.; Stammers, D. K. Structural insights into mechanisms of non-nucleoside drug resistance for HIV-1 reverse transcriptases mutated at codons 101 or 138. *FEBS J.* **2006**, *273*, 3850−3860.
(35) *Maestro*, version 10.2; Schrödinger, LLC: New York, NY, 2015.
(36) Case, D. A.; Betz, R. M.; Cerutti, D. S.; Cheatham, T. E., III; Darden, T. A.; Duke, R. E.; Giese, T. J.; Gohlke, H.; Goetz, A. W.; Homeyer, N.; Izadi, S.; Janowski, P.; Kaus, J.; Kovalenko, A.; Lee, T. S.; LeGrand, S.; Li, P.; Lin, C.; Luchko, T.; Luo, R.; Madej, B.; Mermelstein, D.; Merz, K. M.; Monard, G.; Nguyen, H.; Nguyen, H. T.; Omelyan, I.; Onufriev, A.; Roe, D. R.; Roitberg, A.; Sagui, C.; Simmerling, C. L.; Botello-Smith, W. M.; Swails, J.; Walker, R. C.; Wang, J.; Wolf, R. M.; Wu, X.; Xiao, L.; Kollman, P. A. *AMBER 2016*; University of California: San Francisco, 2016.
(37) Hornak, V.; Abel, R.; Okur, A.; Strockbine, B.; Roitberg, A.; Simmerling, C. Comparison of multiple Amber force fields and development of improved protein backbone parameters. *Protein* **2006**, *65*, 712−725.
(38) Lindorff-Larsen, K.; Piana, S.; Palmo, K.; Maragakis, P.; Klepeis, J. L.; Dror, R. O.; Shaw, D. E. Improved side-chain torsion potentials for the Amber ff99SB protein force field. *Proteins* **2010**, *78*, 1950−1958.
(39) Søndergaard, C. R.; Olsson, M. H. M.; Rostkowski, M.; Jensen, J. H. Improved treatment of ligands and coupling effects in empirical calculation and rationalization of pKa values. *J. Chem. Theory Comput.* **2011**, *7*, 2284−2295.
(40) Wang, J.; Wolf, R. M.; Caldwell, J. W.; Kollman, P. A.; Case, D. A. Development and testing of a general amber force field. *J. Comput. Chem.* **2004**, *25*, 1157−1174.
(41) Wang, J.; Cieplak, P.; Kollman, P. A. How well does a restrained electrostatic potential (RESP) model perform in calculating conformational energies of organic and biological molecules? *J. Comput. Chem.* **2000**, *21*, 1049−1074.
(42) Frisch, M. J.; Trucks, G. W.; Schlegel, H. B.; Scuseria, G. E.; Robb, M. A.; Cheeseman, J. R.; Scalmani, G.; Barone, V.; Mennucci, B.; Petersson, G. A.; Nakatsuji, H.; Caricato, M.; Li, X.; Hratchian, H. P.; Izmaylov, A. F.; Bloino, J.; Zheng, G.; Sonnenberg, J. L.; Hada, M.; Ehara, M.; Toyota, K.; Fukuda, R.; Hasegawa, J.; Ishida, M.; Nakajima, T.; Honda, Y.; Kitao, O.; Nakai, H.; Vreven, T.; Montgomery, J. A., Jr.; Peralta, J. E.; Ogliaro, F.; Bearpark, M.; Heyd, J. J.; Brothers, E.; Kudin, K. N.; Staroverov, V. N.; Kobayashi, R.; Normand, J.; Raghavachari, K.; Rendell, A.; Burant, J. C.; Iyengar, S. S.; Tomasi, J.; Cossi, M.; Rega, N.; Millam, J. M.; Klene, M.; Knox, J. E.; Cross, J. B.; Bakken, V.; Adamo, C.; Jaramillo, J.; Gomperts, R.; Stratmann, R. E.; Yazyev, O.; Austin, A. J.; Cammi, R.; Pomelli, C.; Ochterski, J. W.; Martin, R. L.; Morokuma, K.; Zakrzewski, V. G.; Voth, G. A.; Salvador, P.; Dannenberg, J. J.; Dapprich, S.; Daniels, A. D.; Farkas, Ö.; Foresman, J. B.; Ortiz, J. V.; Cioslowski, J.; Fox, D. J. *Gaussian 09*, revision E.01; Gaussian, Inc.: Wallingford CT, 2009.

DOI: 10.1021/acs.jmedchem.8b01729
J. Med. Chem. 2019, 62, 2083−2098

(43) Jorgensen, W. L.; Chandrasekhar, J.; Madura, J. D.; Impey, R. W.; Klein, M. L. Comparison of simple potential functions for simulating liquid water. *J. Chem. Phys.* **1983**, *79*, 926−935.
(44) Ryckaert, J.-P.; Ciccotti, G.; Berendsen, H. J. C. Numerical integration of the cartesian equations of motion of a system with constraints: molecular dynamics of n-alkanes. *J. Chem. Phys.* **1977**, *23*, 327−341.
(45) Darden, T.; York, D.; Pedersen, L. Particle mesh Ewald: An N·log(N) method for Ewald sums in large systems. *J. Chem. Phys.* **1998**, *98*, 10089−10092.

DOI: 10.1021/acs.jmedchem.8b01729
J. Med. Chem. 2019, 62, 2083−2098